AIAA JOURNAL
Vol. 44, No. 3, March 2006

Toward Validation of Large Eddy Simulation for Turbulent Combustion

Joseph C. Oefelein,* Robert W. Schefer,† and Robert S. Barlow‡
Sandia National Laboratories, Livermore, California 94551-9051

A quantitative overview focused on validation of the large eddy simulation (LES) technique for application to gas-turbine combustion processes is provided. The primary objective is to provide a systematic analysis of the current state of the art and assist in the development of technical performance metrics for model validation. Research is currently required to provide both improved multiphase combustion models and improved datasets for validation. Phenomenological requirements for further model development must be established through more detailed analyses of the space–time characteristics of small-scale turbulence–chemistry interactions. Concurrently, a refined set of implementation requirements must be established for LES, and a systematic hierarchy of databases for model validation must be developed. Steps taken toward these goals are described by focusing on validation requirements, boundary conditions, and the progressive implementation of LES in more complex configurations. First the distinct set of tradeoffs and requirments for LES are listed. A systematic progression of case studies that highlight key aspects related to the state of the art is then presented. In conclusion, recent findings associated with the International Workshop on Measurement and Computation of Turbulent Nonpremixed Flames, from the perspective of validation and model development for LES, are highlighted.

I. Introduction

IMPROVEMENTS in computational speed and capacity over the past several years have made application of the large eddy simulation (LES) technique feasible for increasingly complex flows. This method has been used successfully as both a complementary tool for understanding turbulence and for modeling the effects of turbulence in a variety of engineering applications. With the advent of massively parallel computer hardware, LES now provides a means to study coupled combustion, transport, and multiphase processes in parameter spaces that are unattainable using the direct numerical simulation (DNS) technique, with a degree of fidelity that can be far more accurate than other conventional methods. Here we focus on issues related to the development and application of LES to gas-turbine combustion processes. The primary objective is to provide a systematic analysis of the current state of the art and assist in the development of technical performance metrics for model validation.

Development of next-generation gas-turbine systems requires optimal flowpath integration and thermal management. Flow processes are inherently turbulent, and enhanced performance and operability between the turbomachinery and combustor are imperative for improved control of combustion dynamics over a wide range of operating conditions. Most systems now operate at elevated chamber pressures to enhance performance. This significantly increases the operational Reynolds numbers and turbulence intensities present in various flow passages and the combustion chamber. In many cases, operating pressures approach or exceed the thermodynamic critical pressure of the fuel and/or oxidizer. Under these conditions, many fundamental questions arise regarding the dynamic behavior of the system. A significant shortfall associated with these stringent system requirements is the lack of validated design and analysis tools. These tools are required to achieve optimal control of the highly turbulent and unsteady flowpath dynamics, the fuel-oxidizer mixing characteristics, and the resultant combustion dynamics.

LES provides a means to study coupled mixing and combustion processes with a higher degree of fidelity than conventional methods such as those based on the Reynolds-averaged Navier–Stokes (RANS) approximation. This potential advantage is offset by a much stricter set of developmental and operational requirements. Results from LES are far more sensitive to algorithmic characteristics and boundary conditions. Significant care must be taken to ensure that conservation properties are enforced and that dissipation and dispersion errors do not impose erroneous results. The application of LES also comes with a much stricter set of resolution requirements that cannot be violated. Unlike the RANS approach, which averages over both the temporal and spatial scales, LES maintains both the temporal and spatial characteristics of the turbulence. The assumption that LES accurately captures these dynamic broadband processes must be validated in a manner that quantifies both the temporal and spatial coherence of the flow.

Significant research is required to provide 1) improved multiphase combustion models and 2) improved datasets for validation. Phenomenological requirements for advanced model development must be established through more detailed analyses of space–time characteristics associated with multiscale turbulence–chemistry interactions. Concurrently, a refined set of implementation requirements must be established for LES, and a systematic hierarchy of databases for model validation must be developed. This paper outlines steps taken toward these goals by focusing on three distinct issues:

1) The first issue is validation requirements. The assumption that LES and relevant subgrid-scale closure schemes accurately model the temporal and spatial characteristics of a flow system must be validated with a wide range of simultaneous measurements. Minimal requirements include comparisons of the cold flow characteristics, initial and boundary conditions, time-averaged and unsteady measurements of velocity, and scalar mixing processes. Measurements of unsteady strain, flame structure (curvature, wrinkling, surface area), surface dynamics, and reaction rates are also desirable but not easily measured. Eventually, data sets that characterize flame stability, acoustic interactions, ignition, and extinction phenomena will also be required.

2) The second issue is boundary conditions. Use of experiments that provide clean, nonambiguous boundary conditions are imperative. Both the mean flow quantities and higher time-evolving moments at respective inflow boundaries are required and must be

Received 3 March 2005; revision received 11 May 2005; accepted for publication 10 August 2005.

*Principal Member of Technical Staff, Mail Stop 9051, P.O. Box 969, Combustion Research Facility; oefelei@sandia.gov. Senior Member AIAA.

†Senior Member of Technical Staff, Mail Stop 9051, P.O. Box 969, Combustion Research Facility.

‡Principal Member of Technical Staff, Mail Stop 9051, P.O. Box 969, Combustion Research Facility.

matched identically in the simulation. Rig designs that produce fully developed turbulent profiles with adiabatic or isothermal walls provide the optimal way to meet this requirement. The wall temperature or heat flux profiles must be quantified as a function of space and time when isothermal or adiabatic conditions do not exist. Bounded domains with subsonic flow must also provide a well-defined pressure condition at respective outflow boundaries. This is especially important for swirling, recirculating flows. Given the current status, flow conditions that involve transitional or acoustically excited conditions should be avoided.

3) The third issue is flow complexity. Geometric features associated with various experiments, injection techniques, and ambient conditions each impose a distinct set of turbulence, flow, and thermochemical interactions. These interactions provide progressive levels of coupling between the fluid dynamic, thermodynamic, transport, and chemical processes. Identifying and defining these progressive levels of complexity in well-defined geometries serve as effective ways to assess both model accuracy and inherent model sensitivities.

These issues are addressed by first outlining the distinct set of tradeoffs between LES and RANS to provide a common perspective. We then present a systematic progression of case studies that highlight aspects of each issue and the current state of the art. We conclude by highlighting some of the more recent findings associated with target flames that have been studied as part of the International Workshop on Measurement and Computation of Turbulent Nonpremixed Flames.[1]

II. RANS vs LES

Use of the RANS and unsteady-RANS approximations has historically provided the central basis for engineering design codes throughout industry and government. The primary advantage of RANS is that it requires a minimum of computational resources and facilitates fast solution turnaround times required for most engineering design studies. A disadvantage of RANS, however, is that all of the turbulent motions are modeled; thus, it provides only a bulk approximation of all of the strongly coupled phenomenological interactions that occur over the full range of spatial and temporal scales. The closure is entirely empirical and based exclusively on scaling arguments that apply in the time-averaged limit. RANS predictions of complex systems typically give only qualitative insights. They are highly sensitive to models and model constants, and these constants must be adjusted or tuned for every class of flows.

LES is a much more numerically intensive methodology but offers a higher degree of accuracy in return. For this approach, the large energetic scales are resolved and the subgrid scales are modeled to provide a complete representation of the full range of relevant scales. LES closures are time accurate and the subgrid-scale (SGS) models tend to be more universal. The universal nature of the SGS models significantly reduces the need to tune the model constants. Implementation of the dynamic modeling procedure eliminates the need to use any model constants by effectively converting them to local coefficients in space and time. This enhanced fidelity, however, comes at a significant cost in terms of computational resources and turnaround time.

Compared to RANS, the use of LES imposes an extremely strict set of algorithmic and resolution requirements that must be rigorously enforced. A significant range of energetic scales must be resolved on grids that minimize commutation errors. This has stringent implications regarding the density and quality of grids and the amount of allowable grid stretching that can be used. Numerical dissipation and dispersion errors must also be minimized because they have significantly detrimental effects on SGS models and can negate any effect produced by these models. The presence of these errors depletes energetic turbulence scales at the mid to high wave numbers and consequently competes with the models. When this occurs the SGS models themselves have little or no effect, and the contamination often leads to erroneous conclusions. Solutions based on the RANS approximation are inherently less sensitive to dissipation and dispersion errors because only the largest scales of the flow are represented numerically, and the bulk effects of multiple-time, multiple-length scale interactions are modeled.

Algorithms that employ discretization techniques on collocated grids always require the addition of explicit artificial dissipation terms to provide numerical stability and eliminate odd–even decoupling in pressure. These schemes have historically failed to provide minimal damping and dispersion characteristics appropriate for LES. This is easily shown if one compares the magnitude of the residual associated with the artificial dissipation terms to the residual associated with a given SGS model. The former is always orders of magnitude greater in second-order schemes, and the problem persists for higher-order schemes. Fully implicit or semi-implicit staggered grid algorithms, on the other hand, have been shown to provide acceptable characteristics for LES. The key feature of these algorithms is the use of composite convective difference stencils that are entirely imaginary in complex space.

Three primary issues must be addressed to avoid contamination by numerical errors in LES. The numerical method must provide spatially nondissipative and spectrally clean damping characteristics, the algorithm must provide discrete conservation of mass, momentum, and total energy to avoid the buildup of spurious modes, and high-quality grids must be generated with the appropriate levels of resolution. To date, the algorithmic quality of most of the codes used for validation has not received a sufficient level of attention. Because of the initial emphasis on RANS, algorithms used in many legacy solvers employ highly dissipative and dispersive techniques to provide numerical stability. Although acceptable for RANS, which represents only the largest scales of a flow numerically, these algorithms are typically not appropriate for LES. Analogously, the concept of grid independence differs between the two approaches also.

Achieving grid-independent solutions for RANS calculations is inherently tied to the ability of a given grid system to resolve the largest scales in a flow. For LES, the concept of grid independence is tied to the filter cutoff scale, which must be fixed locally based on physical arguments to ensure that an appropriate range of energetic scales is being resolved. The level of energy that must be resolved varies as a function of the modeling approach and has not been well quantified to date. A general perception is that levels approaching 80% must be achieved. The LES technique itself is fundamentally invalid for cases where the filter cutoff to grid spacing becomes less than one. Values of one imply an implicit filtering process that is inherently tied to the grid and spatial differencing scheme. Values greater than one imply explicit filtering. Our current analyses are limited to implicitly filtered solutions.

III. Approach

A. Theoretical Framework

The case studies presented here were performed using a theoretical–numerical framework developed and validated over the last decade by Oefelein.[2,3] This framework has been optimized to meet the strict algorithmic requirements imposed by the LES formalism and was designed to provide a unified treatment of high-Reynolds-number, high-pressure, real-gas turbulent reacting multiphase flows over a wide Mach operating range (from incompressible, through transonic, to supersonic conditions). We are in the process of establishing a suite of validation studies to be published subsequently.

The theoretical–numerical framework solves the fully coupled conservation equations of mass, momentum, total energy, and species. These equations are coupled with an appropriate equation of state, appropriate treatments of thermodynamic and transport properties, and validated mixing and combining rules for the mixtures of interest to accommodate the most general system. The baseline formulation accommodates a generalized treatment of the equation of state, thermodynamics, transport processes, and chemical kinetics for the full multicomponent system. No assumptions are made regarding the ideality of the mixture state.

For LES applications, the instantaneous conservation equations are filtered, yielding expressions for mass

$$\frac{\partial}{\partial t}(\theta\bar{\rho}) + \nabla\cdot(\theta\bar{\rho}\tilde{\boldsymbol{u}}) = \bar{\dot{\rho}}_s \tag{1}$$

momentum

$$\frac{\partial}{\partial t}(\theta\bar{\rho}\tilde{\boldsymbol{u}}) + \nabla\cdot\left[\theta\left(\bar{\rho}\tilde{\boldsymbol{u}}\otimes\tilde{\boldsymbol{u}} + \frac{\mathcal{P}}{M^2}\boldsymbol{I}\right)\right] = \nabla\cdot(\theta\vec{\bar{\mathcal{T}}}) + \bar{\boldsymbol{F}}_s \quad (2)$$

total energy

$$\frac{\partial}{\partial t}(\theta\bar{\rho}\tilde{e}_t) + \nabla\cdot[\theta(\bar{\rho}\tilde{e}_t + \mathcal{P})\tilde{\boldsymbol{u}}] = \nabla\cdot\left[\theta\left(\vec{\mathcal{Q}}_e + M^2(\vec{\bar{\mathcal{T}}}\cdot\tilde{\boldsymbol{u}})\right)\right] + \theta\dot{\bar{Q}}_e + \dot{\bar{Q}}_s \quad (3)$$

and species

$$\frac{\partial}{\partial t}(\theta\bar{\rho}\tilde{Y}_i) + \nabla\cdot(\theta\bar{\rho}\tilde{Y}_i\tilde{\boldsymbol{u}}) = \nabla\cdot(\theta\vec{\mathcal{S}}_i) + \theta\bar{\dot{\omega}}_i + \bar{\dot{\omega}}_{s_i} \quad (4)$$

The terms θ, $\bar{\rho}_s$, $\bar{\boldsymbol{F}}_s$, $\dot{\bar{Q}}_s$, and $\bar{\dot{\omega}}_{s_i}$ represent the filtered void fraction and spray source terms that account for interphase exchange of mass, momentum, total energy, and species, respectively. The terms $\mathcal{P}$, $\vec{\mathcal{T}}$, $\vec{\mathcal{Q}}_e$, and $\vec{\mathcal{S}}_i$ are respective composite, that is, molecular plus SGS, stresses and fluxes. The terms $\dot{\bar{Q}}_e$ and $\bar{\dot{\omega}}_i$ are the filtered energy and species source terms.

B. SGS Closure

The current baseline SGS closure is obtained using the mixed dynamic Smagorinsky model by combining the models proposed by Erlebacher et al.[4] and Speziale[5] with the dynamic modeling procedure.[6–10] The composite stresses and fluxes in Eqs. (1–4) are given as

$$\vec{\bar{\mathcal{T}}} = (\mu_t + \mu)\frac{1}{Re}\left[-\frac{2}{3}(\nabla\cdot\tilde{\boldsymbol{u}})\boldsymbol{I} + (\nabla\tilde{\boldsymbol{u}} + \nabla\tilde{\boldsymbol{u}}^T)\right] - \bar{\rho}\left(\widetilde{\tilde{\boldsymbol{u}}\otimes\tilde{\boldsymbol{u}}} - \tilde{\tilde{\boldsymbol{u}}}\otimes\tilde{\tilde{\boldsymbol{u}}}\right) \quad (5)$$

$$\vec{\mathcal{Q}}_e = \left(\frac{\mu_t}{Pr_t} + \frac{\mu}{Pr}\right)\frac{1}{Re}\nabla\tilde{h} + \sum_{i=1}^{N}\tilde{h}_i\vec{\mathcal{S}}_i - \bar{\rho}\left(\widetilde{\tilde{h}\tilde{\boldsymbol{u}}} - \tilde{\tilde{h}}\tilde{\tilde{\boldsymbol{u}}}\right) \quad (6)$$

$$\vec{\mathcal{S}}_i = \left(\frac{\mu_t}{Sc_{t_i}} + \frac{\mu}{Sc_i}\right)\frac{1}{Re}\nabla\tilde{Y}_i - \bar{\rho}\left(\widetilde{\tilde{Y}_i\tilde{\boldsymbol{u}}} - \tilde{\tilde{Y}}_i\tilde{\tilde{\boldsymbol{u}}}\right) \quad (7)$$

Here, the term μ_t is the SGS eddy viscosity given by the relation

$$\mu_t = \bar{\rho}C_R\Delta^2\Pi_{\tilde{S}}^{\frac{1}{2}} \quad (8)$$

where

$$\Pi_{\tilde{S}} = \tilde{\boldsymbol{S}}:\tilde{\boldsymbol{S}}, \qquad \tilde{\boldsymbol{S}} = \tfrac{1}{2}(\nabla\tilde{\boldsymbol{u}} + \nabla\tilde{\boldsymbol{u}}^T) \quad (9)$$

The terms C_R, Pr_t, and Sc_{t_i} are the Smagorinsky, SGS-Prandtl, and SGS-Schmidt numbers and are evaluated dynamically as functions of space and time. Thus, there are no tuned constants employed anywhere in the closure. The overall model includes the Leonard and cross-term stresses and provides a Favre-averaged generalization of the Smagorinsky eddy–viscosity model[11] coupled with gradient diffusion models that simulate SGS mass and energy transport processes.

C. Thermodynamic and Transport Properties

The property evaluation scheme is designed to account for thermodynamic nonidealities and transport anomalies over a wide range of pressures and temperatures. This scheme is comprehensive and intricate; thus, only a skeletal description can be given here. The extended corresponding states model[12,13] is employed with a cubic equation of state. In past studies[14,15] modified versions of both the Benedict–Webb–Rubin (BWR) equation of state and cubic equations of state have been used to evaluate the p–v–T behavior of the inherent dense multicomponent mixtures. Use of modified BWR equations of state in conjunction with the extended corresponding states principle has been shown to provide consistently accurate results over the widest range of pressures, temperatures, and mixture states, especially at near-critical conditions. A major disadvantage of BWR equations, however, is that they are not computationally efficient.

Cubic equations of state can be less accurate, especially for mixtures at near-critical or saturated conditions, but are computationally efficient. Experience has shown that both the Soave–Redlich–Kwong (SRK) and Peng–Robinson (PR) equations, when used in conjunction with the corresponding states principle, can give accurate results over a wide range of pressures, temperatures, and mixture states of typical interest. The SRK coefficients are fit to vapor pressure data and, are, thus, more suitable for conditions when the reduced temperature is less than one. The PR coefficients, on the other hand, are more suitable for conditions when the reduced temperature is greater than one. A summary of the cubic equations of state and recommended constants is given by Reid et al. (Ref. 16, Chapter 3).

Having established an analytical representation for real mixture p–v–T behavior, thermodynamic properties are obtained in two steps. First, respective component properties are combined at a fixed temperature using the extended corresponding states methodology to obtain the mixture state at a given reference pressure. A pressure correction is then applied using departure functions of the form given by Reid et al. (Ref. 16, Chapter 5). These functions are exact relations derived using Maxwell's relations (see VanWylen and Sonntag,[17] Chapter 10, for example) and make full use of the real mixture p–v–T path dependencies dictated by the equation of state. Standard state properties are obtained using the databases developed by Gordon and McBride[18] and Kee et al.[19] Chemical potentials and fugacity coefficients are obtained in a similar manner.

Molecular transport properties are evaluated using a procedure directly analogous to that outlined earlier for the thermodynamic properties. Viscosity and thermal conductivity are obtained using the extended corresponding states methodologies developed by Ely and Hanley.[20,21] The mass diffusion coefficients and thermal diffusion coefficients are obtained using the methodologies outlined by Bird et al.[22] and Hirschfelder et al.,[23] in conjunction with the corresponding states methodology proposed by Takahashi.[24]

D. Combustion Closure

With the model framework just described in place, the only remaining terms that need to be closed are the filtered energy and chemical source terms. Unlike the preceding sections where we focused exclusively on a specific set of models directly relevant to the subsequent results, our goal here in to provide a more general perspective on different combustion modeling approaches to augment the subsequent discussion.

Issues related to combustion closures for LES are fairly well known, and a variety of approaches have been taken. Most current SGS models have been carried over from RANS and extended in a way that makes use of the additional information available from LES. All of the current SGS models for combustion are relatively simple due to computational limitations and the long-standing requirement of fast turnaround times for calculations. Approaches aimed at obtaining accurate closure schemes for nonpremixed flames include the assumption of fast chemistry, the assumption of laminar flamelets,[25,26] the conditional moment closure (CMC),[27–29] and probability density function (PDF) transport models.[30–33] Klimenko[34] established the relation between CMC and unsteady flamelets. There are significant tradeoffs associated with each of these approaches:

1) The assumption of fast chemistry, while computationally simple and inexpensive, circumvents the estimation of the chemical source terms. Under this assumption, the thermodynamic state is completely determined as a function of mixture fraction. Effects like ignition and extinction cannot be accounted for, and the formation of pollutants, whose rates of formation are kinetically limited, are poorly predicted.

2) Laminar flamelet models assume that flame structures are thin in comparison to turbulent eddies. The laminar flamelet regime is

considered to comprise an ensemble of strained laminar flames that only depend on mixture fraction and scalar dissipation. Although computationally efficient, there is considerable debate on the degree to which the flamelet assumption is valid at device relevant conditions and the applicability of this method to flames outside of the flamelet regime.

3) The CMC method solves transport equations of conditionally averaged quantities instead of the spatially filtered counterparts. Variables that chemical reactions are known to depend on must be identified and used as conditioning variables. Whereas CMC tends to be more global, solving transport equations in conditioned space adds more dimensions to the problem. With these dimensions come additional modeling issues, approximations, and the related uncertainties.

4) PDF transport methods solve a transport equation for the filtered joint PDF of species, energy, etc., to represent SGS interactions within a statistical hypervolume. The filtered chemical source terms occur in closed form within the transport equation of the joint PDF. The dimensionality, however, increases with the number of species, and issues related to the closure are shifted from treatment of the chemical source terms to modeling unclosed molecular mixing terms.

The limitations just outlined exhibit clear tradeoffs involving model accuracy and the validity of the baseline modeling assumptions. The combustion regime in contemporary devices at atmospheric pressures, for example, is typically intermediate between flamelet combustion and distributed combustion. At elevated pressures the validity of various approximations can change significantly.

Application of the moment-based reconstruction methodology similar to that developed by Pantano and Sarkar[35] and Mellado et al.[36] has the potential to offer a direct method of closing the filtered energy and chemical source terms. Although much more research is required, the conceptual methodology provides the formalism to incorporate progress variable effects directly. The instantaneous scalar field, defined here as the vector $\mathbf{Z} = (p, T, Y_1, \ldots, Y_N)$, is estimated using an approximate deconvolution operation that requires the statistical filtered moments of respective scalars to match to a specified order. The estimated scalar field $\mathbf{Z}_M$ is used as a surrogate for the exact scalar field to calculate the SGS contribution. The surrogate field is given by the expression

$$\mathbf{Z}_M = \bar{\mathbf{Z}} + c_0(\bar{\mathbf{Z}} - \hat{\bar{\mathbf{Z}}}) \tag{10}$$

where $\bar{\mathbf{Z}} = (\bar{p}, \tilde{T}, \tilde{Y}_1, \ldots, \tilde{Y}_N)$ and $\hat{\bar{\mathbf{Z}}}$ represents a test filter value. The coefficient c_0 depends on a modeled spectrum and is a function of the turbulent Peclet number associated with a given scalar $[Re_t(Pr_t \text{ or } Sc_t)]$ and the ratio of the filter length scale to the integral scale of the scalar field γ. The functional dependence of c_0 on these quantities is shown in Fig. 1. Respective turbulent Peclet numbers are given by the mixed dynamic Smagorinsky model, which effectively converts c_0 to a dynamic coefficient in a manner consistent with C_R, Pr_t, and Sc_{t_i}.

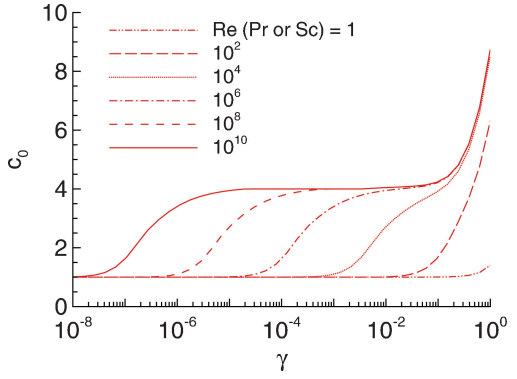

Fig. 1 Functional dependence of c_0 on turbulent Peclet number $[Re_t(Pr_t \text{ or } Sc_t)]$ and ratio of filter length scale to integral scale of scalar field γ.

Modeling premixed flames poses an additional set of constraints. Reaction zones in premixed flames are typically orders of magnitude smaller than the local LES cutoff scale. Chemical reactions occur completely at the SGS level and must be modeled entirely. Examples of recent models include the thickened flame approach,[37] the linear eddy model (LEM),[38] and the level-set G-equation approach.[26] All of these models explicitly assume a flame topology:

1) The thickened flame model artificially increases the characteristic flame diffusivity such that the flame zone is resolved numerically. This introduces errors in the flame propagation speed that must be compensated for by modifying the mean chemical source term. The disadvantage of this approach is that it alters the natural physical coupling between transport and chemical kinetics.

2) The multiple-scale approach simulates spatial and temporal dynamics of SGS scalar mixing and combustion processes using the one-dimensional stochastic methodology provided by LEM.[39] This approach, and its successor, the one-dimensional turbulence model,[40] provide key dynamic information and, thus, have the potential to provide a high-fidelity closure. Current disadvantages are the potential cost and uncertainties related to the SGS to resolved-scale coupling procedure.

3) The G-equation approach applies a level-set procedure to describe the turbulent flame front. The flame front is represented by an arbitrary isosurface of the scalar field defined by G. This isosurface is the only valid quantity, and the evolution equation for G is not uniquely defined and completely empirical in nature. Because of this empiricism, phenomena such as local flame speeds are difficult to quantify.

Models based on assumed flame topologies significantly limit the predictive nature of simulations when the exact regime of combustion is not known a priori. This is always the case for applications that involve swirling and recirculating flow, in which significant variations in thermodynamic and transport properties, turbulence–chemistry interactions, and acoustic interactions can occur locally. To approach a truly predictive capability, next-generation SGS models must incorporate more general closure schemes. Achieving this requires development of detailed validation data sets, close coupling between experiments and simulations, and development of refined criteria with respect to implementation requirements for LES.

E. Numerical Framework

Case studies presented in subsequent sections were performed using a single unified numerical framework. The formulation treats the fully coupled compressible conservation equations but can be evaluated in the incompressible limit. Thus, incompressibility is treated as a limiting extreme of the more general compressible equation set given by Eqs. (1–4). A unique dual-time multistage scheme is employed with a generalized (pseudotime) preconditioning methodology that optimally treats convective, diffusive, geometric, and source term anomalies in a unified manner. The spatial scheme employs a staggered methodology in generalized curvilinear coordinates that provides nondissipative spectrally clean damping characteristics and discrete conservation of mass, momentum, and total energy. This is a critically important feature for LES. The differencing methodology also includes appropriate switches to handle shocks, detonations, flame fronts, and/or contact discontinuities in a manner appropriate for LES.

The baseline method provides a fully implicit time advancement using a fully explicit multistage scheme in pseudotime. The implicit formulation is A stable, which allows one to set the physical time step based solely on accuracy considerations. It accommodates any arbitrary equation of state, handles the thermodynamic nonidealities and transport anomalies over a wide range of conditions typically encountered in contemporary propulsion systems, and provides full thermophysical coupling (compressible and incompressible) over a wide range of conditions. A Lagrangian–Eulerian formulation is employed to accommodate particulates, sprays, or Lagrangian-based combustion models, with full coupling applied between the two systems. The Lagrangian solver can accommodate both particles

and parcel methods and employs asynchronous multiple timescale integration to account efficiently for time-history effects.

The algorithm has been optimized to provide excellent parallel scalability attributes using a distributed multiblock domain decomposition with a generalized connectivity scheme. Distributed-memory message-passing is performed using message passing interface and the single-program–multiple-data model. It accommodates complex geometric features and time-varying meshes with generalized hexahedral cells while maintaining the accuracy of structured spatial stencils. The software package has been ported to all contemporary massively parallel computer platforms. The basic method is well suited for high-performance computations and maintains highly efficient fine-grain scalability attributes.

IV. Case Studies

Here we present a progression of case studies with increasing complexity. Emphasis is placed on validation requirements and implementation of the LES methodology in a manner that minimizes ambiguities associated with the treatment of boundary conditions. Establishing these criteria is a first and necessary step before the more intricate issues related to combustion modeling can be addressed. We conclude by highlighting some of the more recent findings associated with experiments being conducted in the Turbulent Combustion Laboratory at Sandia National Laboratories, in particular, those associated with the Sandia piloted flames and the International Workshop on Measurement and Computation of Turbulent Nonpremixed Flames.[1]

A. Turbulent Channel Flow

Gas-turbine combustion processes are dominated by both the upstream injection characteristics and the downstream pressure distribution at the combustor exit. The injection of air into the chamber through, for example, swirl-cup injectors, always involves strongly coupled fluid dynamic interactions in regions of high shear where the fluid expands into the chamber from the injector ducts. The fluid entering the chamber from the injector is initially dominated by wall-induced shear and the related turbulent boundary-layer interactions. On expansion into the chamber, a transition occurs to a condition that is dominated by free shear-layer interactions. The spatial evolution of the turbulent flow during this transition is governed by small-scale vortical interactions between structures initially created by the injector walls. These structures subsequently coalesce within the free shear-layer just downstream of the injector and grow in a spatially evolving manner. In general, these dynamics must be resolved to represent accurately the evolution of the energetic scales in the combustor.

The limitations of LES in the vicinity of walls are well known. Given these limitations, there are only two basic options available to handle wall effects. The first is to apply one of a variety of wall modeling approaches. The second is to perform a so-called wall-resolved LES by applying near-DNS resolution in the wall-normal direction and maintaining fairly stringent spacing requirements for LES in the streamwise and cross-stream directions. Application of wall models is ultimately the more desired solution because this facilitates significantly coarser grid resolution. The current difficulty, however, is that wall modeling for LES is still in the research stages. It is not clear how accurately these models can represent the turbulent flow dynamics in the vicinity of the injector exit, where the boundary-layer dynamics interact strongly with the downstream shear layer as the fluid expands into the chamber. Application of the wall-resolved approach, on the other hand, is numerically expensive but has proven to provide a reasonably accurate representation of the near-wall turbulence structure when the dynamic modeling procedure is used.

To demonstrate the level of accuracy achieved using the wall-resolved approach, we have performed a validation study by comparing results from an LES, using the theoretical–numerical framework described in the preceding section, to the DNS data provided by Moser et al.[41] Moser et al. have performed DNS calculations of a turbulent channel flow up to a Reynolds number based on the friction velocity of $Re_\tau = 590$. The LES calculations were performed on a grid that was 10^6. The computational domain was $6h \times 2h \times 3h$ in the streamwise, wall-normal, and cross-stream directions, respectively. Stretching was applied in the wall-normal direction such that the first cell from the wall was within a y^+ value of 1 and the first 16 cells within the interval $0 < y^+ < 30$. The transverse grid spacing was set such that Δx^+ and Δz^+ were approximately 50. No-slip boundary conditions were applied at the upper and lower walls, with periodic conditions applied in the streamwise and spanwise directions.

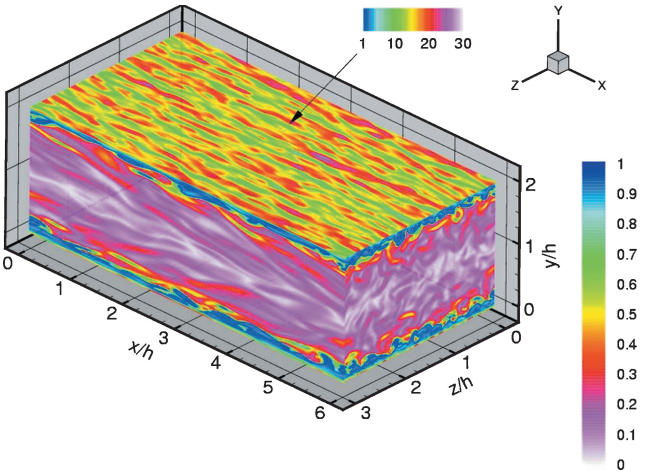

Fig. 2 Instantaneous magnitude of vorticity (dimensionless) from LES of turbulent channel flow at conditions identical to DNS in Ref. 41; Reynolds numbers based on h and friction velocity are $Re_h = 1.38 \times 10^4$ and $Re_\tau = 5.9 \times 10^2$, respectively.

Figure 2 shows a representative result for a Reynolds number based on the friction velocity of $Re_\tau = 590$. This Reynolds number is the highest considered by Moser et al. and coincides with values that typically exist in simple laboratory-scale injector ducts at atmospheric pressure. Shown in Fig. 2 are contours of the instantaneous (dimensionless) magnitude of vorticity. Contour ranges are set to highlight both the structure of the core flow and the longitudinal vortical streaking near the wall. The dimensionless magnitude is observed to vary between 0 and 1 in the core flow and approaches values of 30 near the wall. The longitudinal, cross-stream, and near-wall structure is indicative of the well-known horseshoe vortex dynamics that occurs in turbulent boundary layers, where longitudinal near-wall vortices coalesce in the core flow forming strong cross-stream vorticity components.

Figure 3 shows comparisons of 1) the mean streamwise component of velocity, 2) the streamwise and wall-normal rms components, and 3) the resolved-scale shear stress for the Moser et al. $Re_\tau = 590$ case. The LES results match the DNS data to within 5% or better. This level of agreement is considered necessary to achieve realistic near-wall flow dynamics inside the injector ducts of gas turbines. The results shown in Figs. 2 and 3 are unique in that the solution was obtained by solving the full-compressible conservation equations of mass, momentum, and total energy in the incompressible limit using a time-step based on the convective velocity. In addition to demonstrating an ability to run the full compressible equation set efficiently in the incompressible limit, these data provide a baseline criteria with respect to the resolution required to perform an accurate wall-resolved LES of fully developed turbulence in a duct as a function of the Reynolds number.

B. Particle-Laden Flow in a Coannular Combustor

To build on the criteria established in the preceding subsection, we now focus on the next level of complexity. Sommerfeld and Qui,[42] Sommerfeld et al.,[43] and Sommerfeld and Qui[44] provide a detailed series of one-component phase-Doppler-anemometer (PDA) measurements from a swirling particle-laden flow. A schematic of the experimental apparatus is shown in Fig. 4. The model combustion chamber is designed to produce the classical recirculating flow

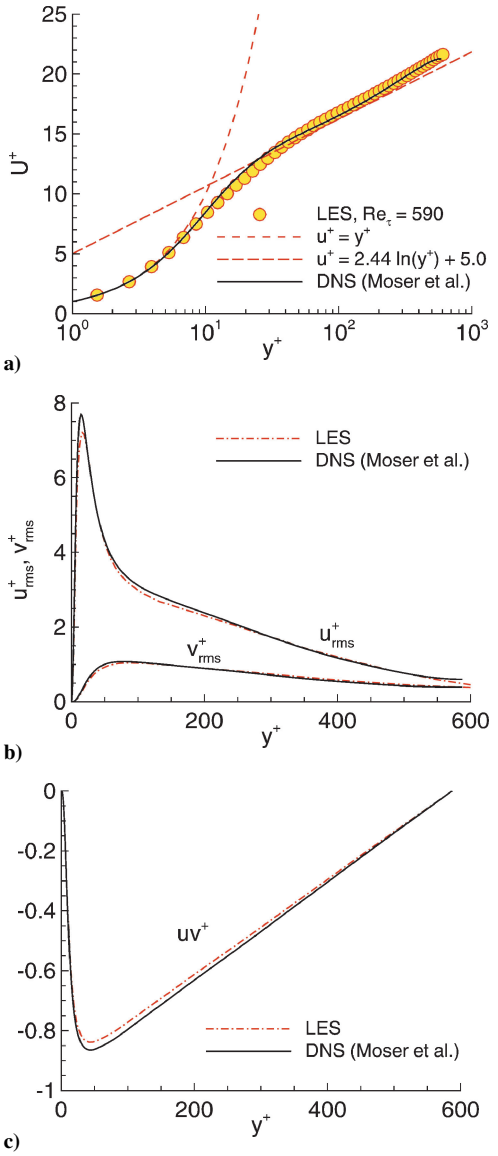

Fig. 3 Time-averaged velocity profiles: a) mean streamwise component, b) streamwise and wall-normal rms components, and c) resolved-scale compared with DNS by Moser et al.[41]

conditions typically observed in gas-turbine combustors. The apparatus is cylindrical and consists of an injector section, main chamber, and plenum chamber. The coannular injector houses a centered particle-laden primary jet surrounded by a swirling secondary jet. Flow is injected into the main chamber from the top. On entering the chamber the flow undergoes a sudden expansion followed by a series of complex fluid dynamic interactions. The flow then undergoes a second expansion at the exit of the main chamber into a plenum chamber. The rig stands vertically, with gravity acting in the downward direction.

The experimental geometry is characterized in dimensionless units using the radius of the outer wall of the secondary jet, $R = 32$ mm, which is also the diameter of the primary jet. The main chamber is approximately 30 dimensionless units in length and extends a radial distance of approximately 3 dimensionless units. The injector section (not completely shown in Fig. 4) extends eight units upstream from the main chamber face plate. The plenum chamber begins approximately 30 dimensionless units downstream of the main chamber, ends at 50 dimensionless units, and extends a radial distance of 9 units. The region of interest bracketed in Fig. 4 is shown in greater detail in Fig. 5. The primary jet has a radius of $r/R = 0.5$ and is laden with spherical glass beads. Flow from the primary jet evolves to a fully developed turbulent state before injection and enters the main chamber axially. The secondary jet extends over a radial interval of $0.59 \leq r/R \leq 1$, is fully developed axially, and is injected into the main chamber with a swirling azimuthal velocity component.

The eight axial stations where cross-sectional PDA measurements were made are also shown in Fig. 5. Gas-phase and particle-phase mean and rms velocity components are given with simultaneous measurements of the particle size and mass flux distributions. Data were obtained with two different particle mass loadings in the primary jet, for three different particle size classes. The relevant flow conditions and particle properties are listed in Table 1. The Reynolds numbers in both the primary and secondary jets are comparable to that in the channel flow presented in the preceding section. Particles are injected into the primary jet in equilibrium with the gas-phase velocity according to the distribution given by Fig. 6. This distribution produces a mean number diameter of 45 μm and particle sizes over the range $20 \leq d_p \leq 80$ μm, which is representative of typical fuel drop size distributions in gas-turbine combustors.

The data acquired by Sommerfeld and Qui,[42] Sommerfeld et al.,[43] and Sommerfeld and Qui[44] provide two excellent benchmark cases

Table 1 Flow conditions and particle properties used in the Sommerfeld experiments

Conditions and properties	Case 1	Case 2
Gas (air)		
Flow rate in primary jet, g/s	9.9	6.0
Flow rate in secondary jet, g/s	38.3	44.6
Inlet Reynolds number[a]	26,200	27,250
Swirl number	0.47	0.49
Temperature, K	300	300
Particle		
Loading ratio in primary jet	0.034	0.17[b]
Flow rate, g/s	0.34	1.0
Mean diameter, μm	45.5	45.5
Density ratio ρ_p/ρ_f	2,152	2,152

[a]Based on total volume flow rate. [b]Five times case 1.

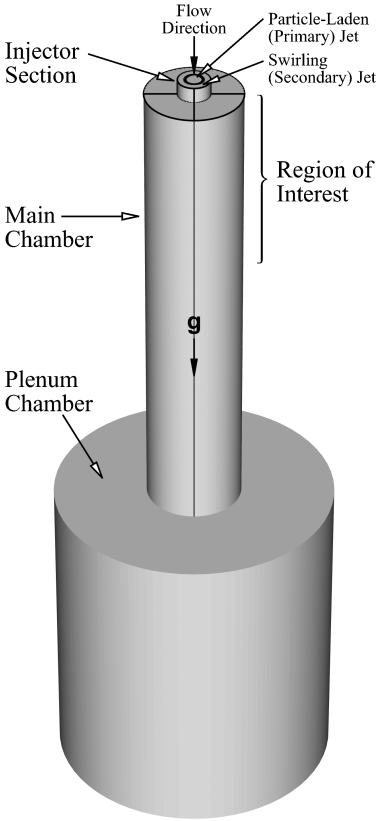

Fig. 4 Schematic of experimental apparatus employed in Refs. 42–44.

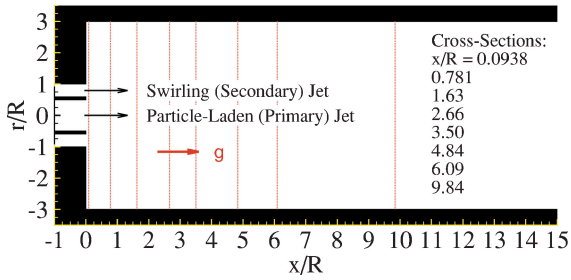

Fig. 5 Region of interest showing location where cross-sectional PDA measurements were made.

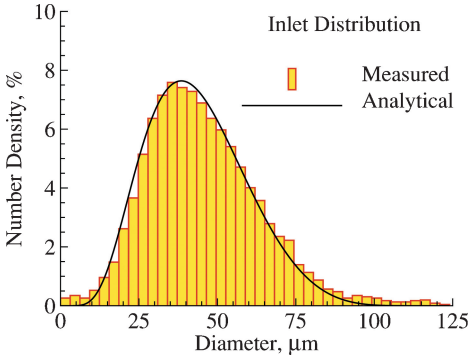

Fig. 6 Particle size distribution in axial (primary) jet.

for validation of LES in a turbulent swirling-flow environment very similar to the flow in a gas-turbine combustor, under highly controlled conditions, and with well-defined boundary conditions. They also provide a way to systematically validate LES of dilute particle dynamics in these flow environments without having to treat the more complex issues associated with atomization, secondary breakup, and coupling between the gas and particulate phases under highly loaded conditions. Establishing this level of validation represents the next progressive step before treating these more daunting issues. To establish this next level of validation, we have performed LES calculations of the Sommerfeld and Qui,[42] Sommerfeld et al.,[43] and Sommerfeld and Qui[44] cases using the theoretical–numerical framework described earlier. Here, our emphasis is on implementation of boundary conditions and the near predictive nature of the subsequent results.

There are three critical issues that must be addressed regarding the implementation of boundary conditions. First, the boundary-layer dynamics inside of the injector ducts must be resolved such that the energetic scales near the wall, that is, where the maxima in the rms velocity and shear stress occur in Fig. 3, provide realistic vortical interactions. Second, the inflow conditions must be generated in a manner that allows the injected jets to interact with the regions of high-shear on entering the main chamber, that is, they must facilitate realistic turbulent fluid interactions inside the shear-layers created by the jets and recirculating flow in the main chamber. Last, the unsteady pressure distribution across the exit plane of the main chamber must be represented in a highly accurate manner. This distribution has a significant influence on the upstream recirculation zones that form in the main chamber, and it is imperative from a validation perspective that these zones be reproduced accurately. To address these issues, the computational domain used for the LES was designed to match identically the experimental domain shown in Fig. 4.

The grid used to perform the calculations includes the injector section, main chamber, plenum chamber, and the portion of the injector section not shown in Figs. 4 and 5, which places the inlet plane of the primary and secondary jets at a location of eight dimensionless units upstream of the entrance to the main chamber. This added portion provides the appropriate development lengths required to drive fully developed turbulent flow in both ducts. The grid spacing in the primary and secondary jets were set by adhering to the resolution requirements established in the preceding section for the channel- flow case. The azimuthal grid spacing was set using a uniform distribution of 64 cells. The grid density in the primary jet was set at $128 \times 64 \times 64$ in the axial, radial, and azimuthal directions, respectively. Similarly, the grid density in the swirling secondary jet was set at 128×128. This resolution provides the same level of fidelity in each of the ducts as achieved for the channel flow calculation in the last section; that is, the first cell from the wall was within a y^+ value of 1, the first 16 cells were within the interval $0 < y^+ < 30$, and the transverse grid spacing was set such that Δx^+ and Δz^+ where both less than 50.

The grid for the main chamber was constructed using the resolution requirements in the injector ducts as a baseline. The axial grid distribution was set by matching the spacing of adjacent cells in the injector section and stretching from the entrance of the main chamber (where the flow enters from the injector) to the exit (where the flow is further expanded into the plenum). Stretching was accomplished by maintaining a relative stretching factor of 1.02 between adjacent cells. The grid spacing in the radial direction was set by matching the radial distributions of the cells in the injector ducts at the inlet and filling in the remaining area in a manner by reflecting the stretching functions on adjacent sides of the ducts. The spacing on the plenum side of the main chamber was set to be uniform, with the inner distribution smoothly transitioned between these two endpoints. The resultant grid density is $128 \times 288 \times 64$.

The expansion induced by the plenum chamber has a significant influence on the upstream recirculation zones that form in the main chamber. It is imperative that this section be included as part of the LES calculation to provide the correct unsteady pressure distribution across the exit plain of the main chamber. Significant errors can occur otherwise because a change in the overall structure of the recirculation zones induces a global shift in the location of the mean flow characteristics. Such a shift makes comparisons between measured and modeled results meaningless. The grid density in the plenum itself can be fairly coarse. Here, we match the grid at the exit of the main chamber and stretch such that the entire plenum region is filled with a $32 \times 296 \times 64$ grid. The final grid of the entire domain is constructed with 1.5, 2.3, and 0.6 million cells in the injector section, main chamber, and plenum chamber, respectively.

It is extremely difficult to specify a complete time-accurate description of the resolved-scale component of velocity, as required by Eq. (2), because this quantity is entirely dependent on the filter cutoff value and grid. The best strategy to simulate these quantities accurately in a manner that provides both realistic boundary-layer dynamics and turbulent fluid interactions on injection into the main chamber is to include the injector configuration and appropriate upstream development lengths directly into the calculation. This is a critical factor that must be considered in the design of any experiment intended for validation purposes.

The Sommerfeld apparatus (see Refs. 42–44) provides a particularly simple way to impose the upstream boundary conditions. The injector section is long enough that it is valid to assume fully developed turbulent profiles exist at the inlet to the computational domain just described. With the added assumption that all wall surfaces are hydraulically smooth, we can use the LES solver itself to drive fully developed turbulence in the injector ducts. The procedure is shown for the swirling secondary jet in Fig. 7. Fully developed turbulent velocity profiles are generated inside the injector ducts by recycling the unsteady velocity field from radial planes at an axial distance of two dimensionless units upstream of the main chamber face plate. The structure of resolved-scale turbulence generated in the ducts is identical to that shown in Fig. 2. The stripped fields are corrected to maintain the mass flow rates specified in Table 1, then imposed at the injector inlet eight units upstream with a nonreflecting pressure condition. The secondary jet is also corrected by modulating the azimuthal velocity in a manner that produces the correct experimentally measured swirl number at the injector exit. The latter operation is done using a simple control loop that converges on

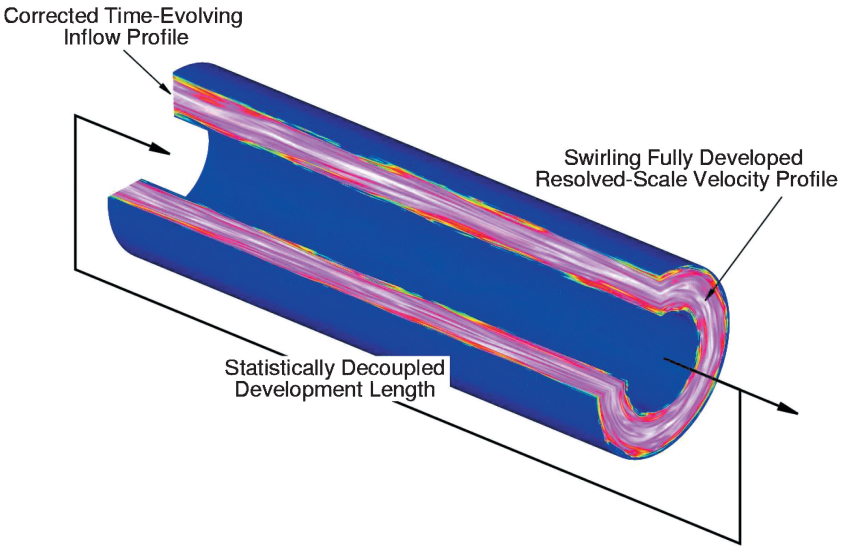

Fig. 7 Implementation of upstream boundary conditions in injector section.

the azimuthal component of velocity required at the inlet to produce the preselected swirl numbers at the injector exit. All of the walls inside the injector ducts are assumed to be adiabatic. The walls in the main chamber are assumed to be 300 K.

To handle the particulate phase, Lagrangian particle models for momentum are employed using the fundamental framework developed by Oefelein.[14] The source term $\bar{\boldsymbol{F}}_s$ in Eq. (2) accounts for the interphase exchange of momentum imposed by the particles on the resolved scales. For particles on the order of, or smaller than, the Kolmogorov scale, this term is given by an expression of the form

$$\bar{\boldsymbol{F}}_s(\boldsymbol{x},t) = \underbrace{\int_t^{t+\Delta t} \underbrace{\sum_p \mathcal{G}(\boldsymbol{y}_p - \boldsymbol{x}, \tau - t) \underbrace{\left\{ m_p \frac{\mathrm{d}\boldsymbol{u}_p}{\mathrm{d}\tau} \right\}}_{\text{(i)}}}_{\text{(ii)}} \mathrm{d}\tau}_{\text{(iii)}} \tag{11}$$

Here the quantity $\mathcal{G}$ denotes a generic filter function which characterizes the influence of SGS dynamics at remote points $(\boldsymbol{y}, \tau)$ on resolved-scale values at $(\boldsymbol{x}, t)$. Term (i) in Eq. (11) represents the instantaneous force induced by respective particles at remote points $\boldsymbol{y}_p$ and times τ. Term (ii) represents the spatially filtered effect of these remote exchange processes on discrete points $\boldsymbol{x}$ within the volume of influence defined by the filter. Term (iii) represents the filtered effect of SGS temporal disturbances over the integration time-step $\delta\tau$.

In this study, the governing conservation equations are filtered implicitly, and the resolved-scale variables represent volumetric averages based on the spectral characteristics of the staggered second-order stencils. The particle source in cell methodology[45] is applied at respective cell centroids in a manner consistent with the staggered scheme. For this situation, the term

$$\sum_p$$

in Eq. (11) represents a summation over all discrete particles within a given finite volume cell. This approximation was found to be acceptable for the cases considered here because the particle loading is almost negligible.

Particle dynamics are simulated assuming that 1) the density of the particles is much greater than the density of the carrier fluid, 2) the particles are dispersed and collisions between particles are negligible, 3) the particles are on the order of, or smaller than, the Kolmogorov scale in size, and 4) that particle motion due to shear is negligible. Under these assumptions, the Lagrangian equations that govern instantaneous particle motion can be written as

$$\frac{\mathrm{d}\boldsymbol{x}_p}{\mathrm{d}\tau} = \boldsymbol{u}_p \tag{12}$$

$$\frac{\mathrm{d}\boldsymbol{u}_p}{\mathrm{d}\tau} = \frac{\tau_f}{\tau_r}(\boldsymbol{u} - \boldsymbol{u}_p) + \frac{R}{U^2}\boldsymbol{g} \tag{13}$$

These equations are nondimensionalized using the same reference quantities used in Eqs. (1–4). The subscript p denotes values associated with individual fluid particles. The ratio τ_r/τ_f (where $\tau_f = R/U_{\text{ref}}$) is the dimensionless particle relaxation time

$$\tau_r/\tau_f = \mathrm{St}\Big/\left(1 + a_p Re_p^{b_p}\right) \tag{14}$$

The term St is the Stokes number based on the mean flow timescale τ_f, that is,

$$\mathrm{St} = \tau_p/\tau_f = (1/18)\rho_p d_p^2 Re \tag{15}$$

The quantities ρ_p and d_p are the dimensionless particle density and diameter, respectively. The term Re_p is the particle Reynolds number

$$Re_p = d_p Re|\boldsymbol{u} - \boldsymbol{u}_p| \tag{16}$$

The instantaneous drag acting on respective particles is modeled using the nonlinear correlation given by Schiller and Nauman (see Ref. 46). With this correlation, Eq. (14) is evaluated using $a_p = 0.15$ and $b_p = 0.687$. This correlation matches the standard drag curve to within $\pm 4\%$ on the interval $Re_p < 800$. Equations (12) and (13) are integrated using a fourth-order Runge–Kutta time-stepping technique applied in a manner consistent with the evaluation of the explicit terms in the gas-phase solver. Trilinear interpolation of the resolved-scale velocity components is combined with a Langevin model to simulate SGS dispersion processes.[14,47] Two-way coupling is achieved by simultaneously evaluating the source terms given by Eq. (11) and the individual contributions imposed by term (i) in Eq. (11).

A representative LES solution corresponding to case 2 in Table 1 is shown in Fig. 8. Figure 8 shows the instantaneous particle distribution superimposed on the corresponding turbulent velocity field. The radial cross sections correspond to the eight axial stations where PDA measurements were made and clearly highlight the asymmetric precessing nature of the flow. At any instant in time there are approximately 2.5 million particles being tracked in the region of interest. Tracking this number of particles is significant because it verifies

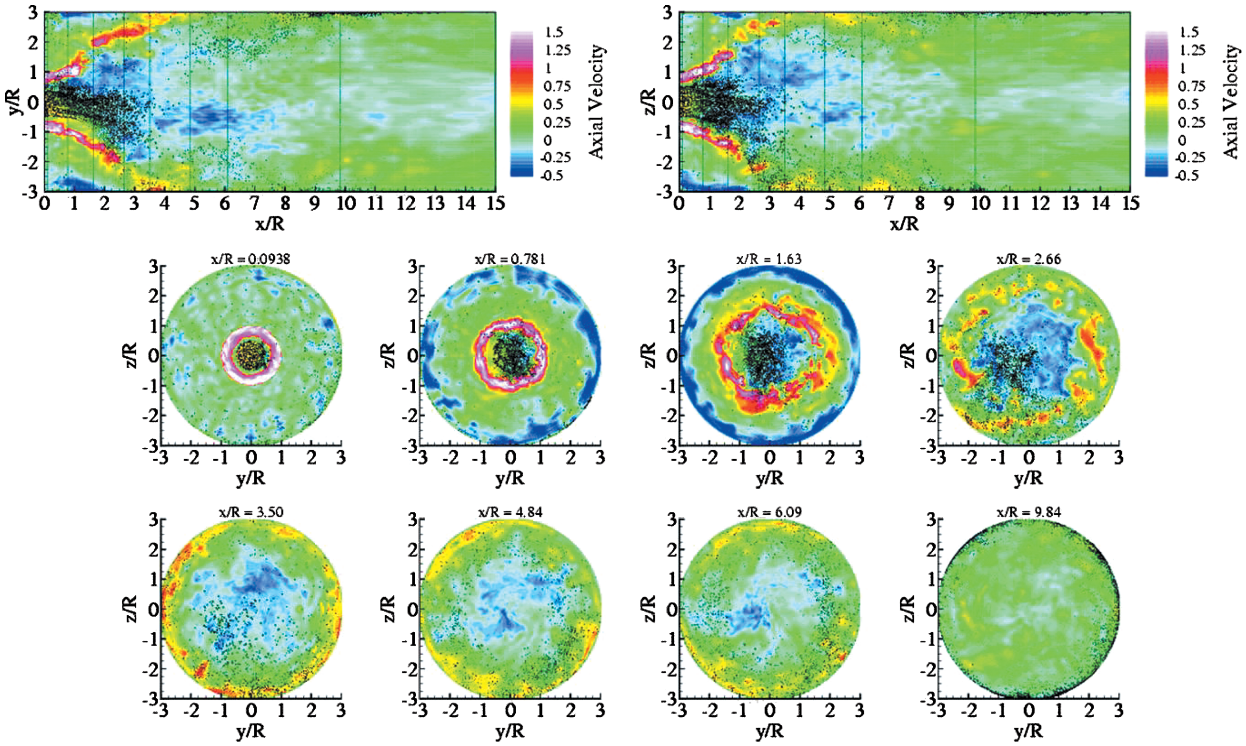

Fig. 8 Instantaneous particle distribution superimposed on corresponding turbulent velocity field (case 2); cross sections correlate with axial locations shown in Fig. 5.

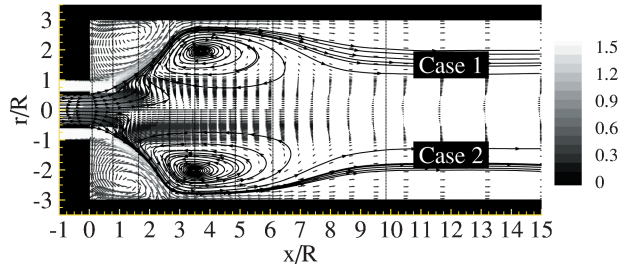

Fig. 9 Time-averaged flow characteristics associated with case 1 and case 2.

the feasibility of employing large numbers of physical particles and eliminates the need to implement classical parcel approximations.

The mean flow characteristics are given in Fig. 9, which shows the time-averaged gas-phase velocity field for both case 1 and case 2. With the focus first on case 1, key features of the flow include the primary and secondary recirculation zones with cores centered at the $(x/R, r/R)$ coordinates of (3.7, 2.0) and (1.4, 2.4), respectively; the stagnation point in the core region centered at approximately (3.3, 0.0); and the reattachment point centered at approximately (2.5, 3.0). These numbers coincide with the measured results reported by Sommerfeld (see Refs. 42–44) to within 5%. The highest negative velocities within the primary recirculation bubble are found at the coordinates (3.7, 1.1). Comparing the characteristics between cases 1 and 2 highlights the effect of particle loading on the mean flow characteristics. Particles, which initially have the same velocity as the air, are not able to follow the rapid expansion and deceleration of the gas jets on injection into the main chamber and tend to have a higher velocity in the core region. The larger particles have the highest velocities and tend to penetrate the central reverse flow region. The smaller particles, on the other hand, tend to respond quickly to the recirculation of the gas flow and are more prone to entrainment in the secondary recirculation zone. Increasing the particle loading tends to increase the momentum in the primary recirculation zone such that the gas-phase flow penetrates to a lesser extent.

Direct comparisons between measured and modeled results for case 2 are shown in Figs. 10–14. Results in each of Figs. 10–14 coincide with the experimental measurement locations shown in Fig. 5. Figures 10 and 11 show comparisons of the mean and rms components of the axial, radial, and azimuthal components of velocity. Open circles represent the measured data acquired by Sommerfeld and Qui,[42] Sommerfeld et al.,[43] and Sommerfeld and Qui,[44] and the lines represent time-averaged LES results. Identical comparisons for the particle-phase are given in Figs. 12 and 13. Figure 14 shows comparisons between the particle diameter (both mean and rms profiles) and the momentum flux profiles. These data represent a small subset of the available results and provide a reasonable representation of the level of accuracy achieved in the simulations. In all cases, the agreement between the measured and calculated results is excellent. We achieve the best agreement on the gas-phase mean values, which clearly falls within the experimental error bounds. Similar agreement is achieved with respect to the gas-phase rms values, with only slight degradation compared to the mean values. Comparisons between the particle-phase quantities are not quite as good, but exhibit similar trends and are still well within the experimental uncertainties.

The agreement between the measured and modeled results exhibited in Figs. 10–14 is especially significant because there are no tuned constants used in any of the models. The only controlling parameters in the simulation are the grid spacing and implementation of boundary conditions. Thus, discrepancies can only be attributed to four possibilities: 1) bad numerics, 2) lack of appropriate grid resolution, 3) ill-posed implementation of boundary conditions, or 4) poor model performance. By implementing the approach just described, we are able to eliminate fairly confidently all but the last before performing the calculation. We can further conclude, based on the agreement between the measured and model results, that the current modeling approach performs relatively well for multiphase flow under lightly loaded conditions and approaches a predictive capability for the conditions cited.

The novel feature of the results shown is that the cases studied allowed us to establish a baseline level of confidence in our ability to simulate a complex flows at conditions representative of

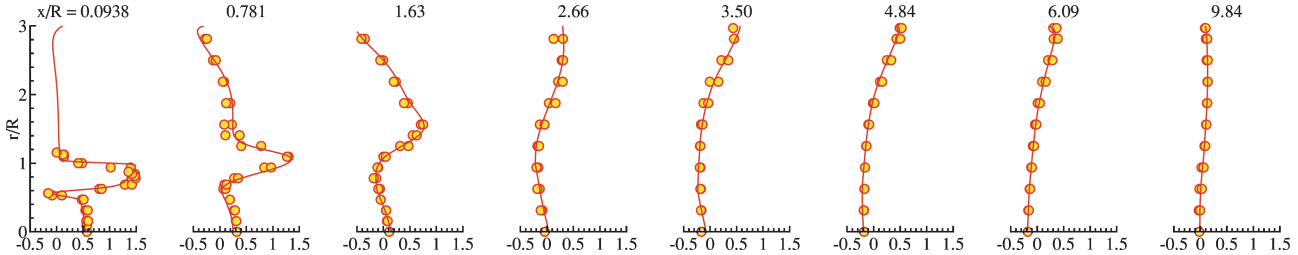

a) Axial component

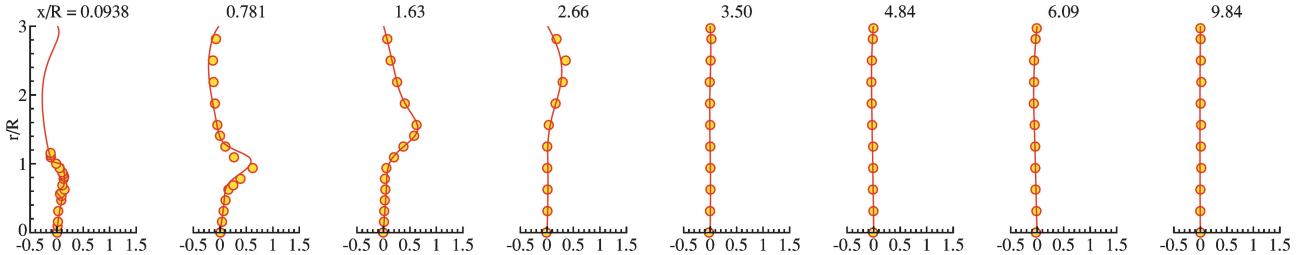

b) Radial component

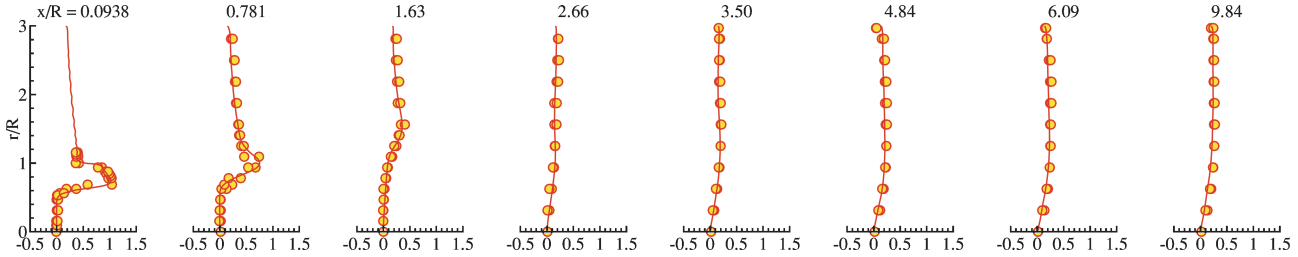

c) Azimuthal component

Fig. 10 Time-averaged profiles of dimensionless gas-phase velocity field (case 2): ○, measured data from Refs. 42–44 and ——, LES results.

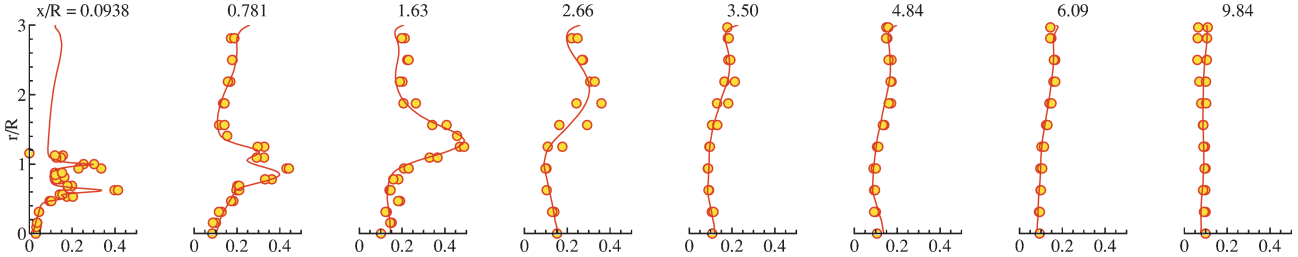

a) Axial component

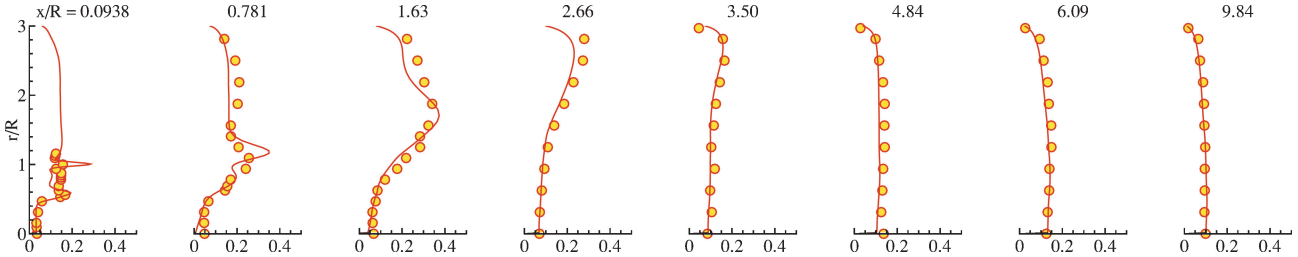

b) Radial component

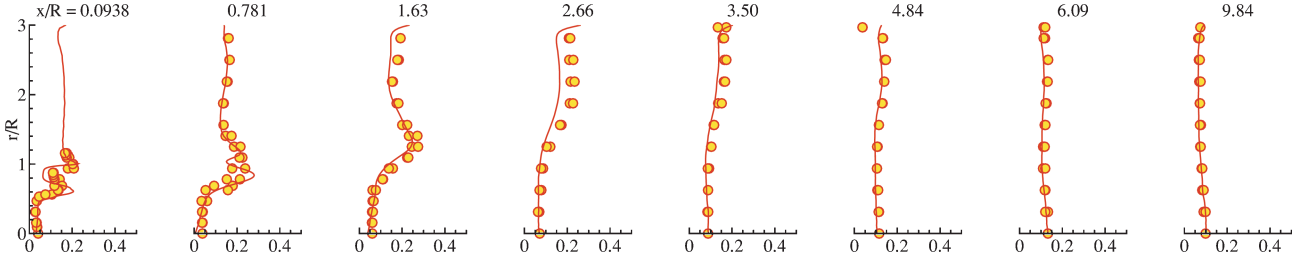

c) Azimuthal component

Fig. 11 RMS profiles of dimensionless gas-phase velocity field (case 2): ○, measured data from Refs. 42–44 and ——, LES results.

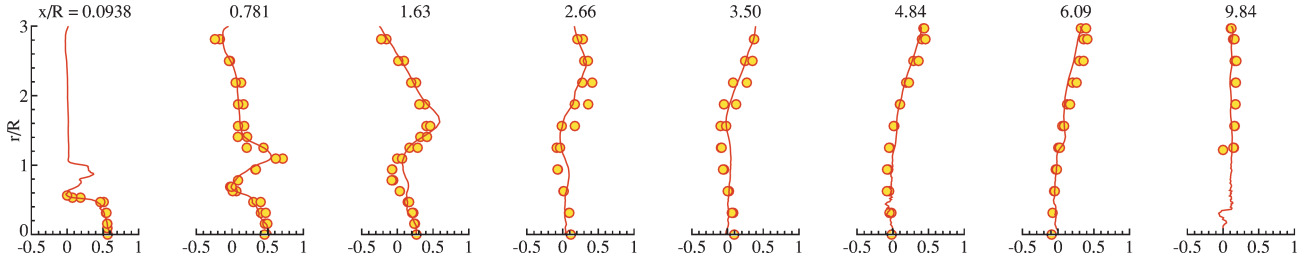

a) Axial component

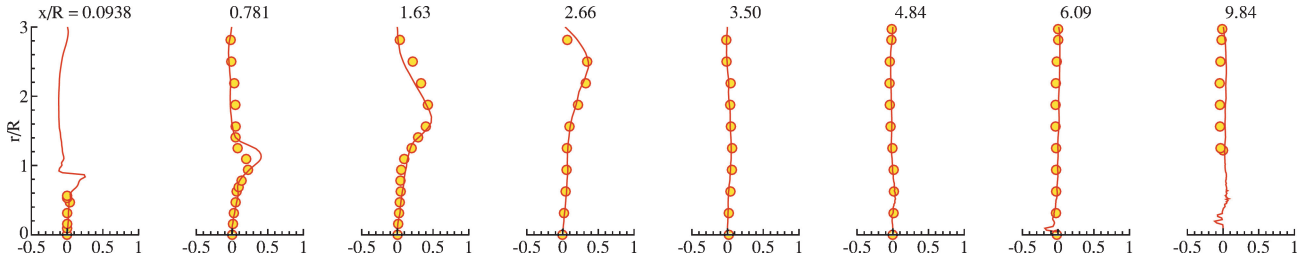

b) Radial component

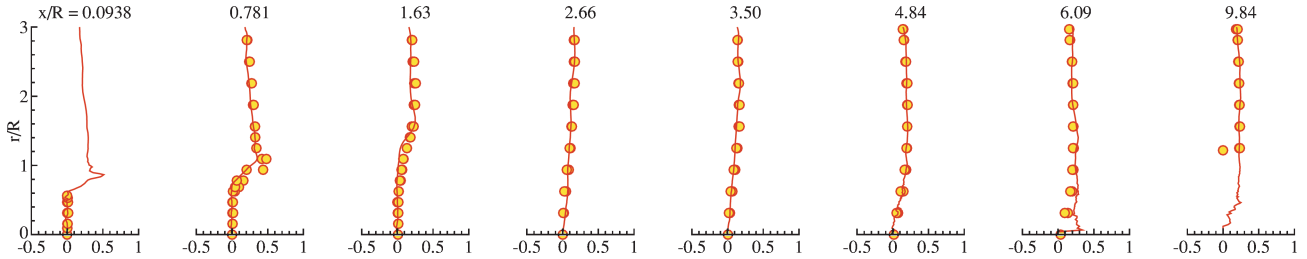

c) Azimuthal component

Fig. 12 Time-averaged profiles of dimensionless particle-phase velocity field (case 2): ○, measured data from Refs. 42–44 and ——, LES results.

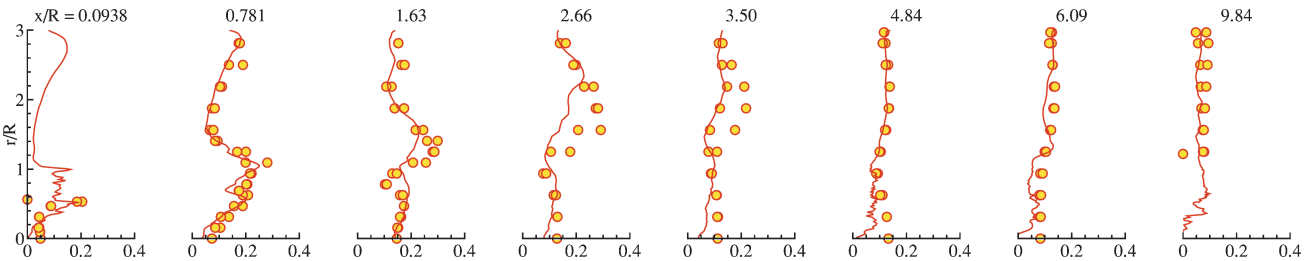

a) Axial component

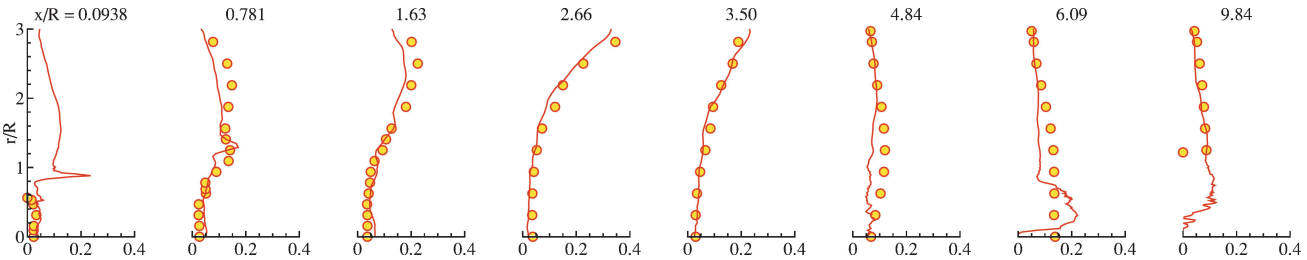

b) Radial component

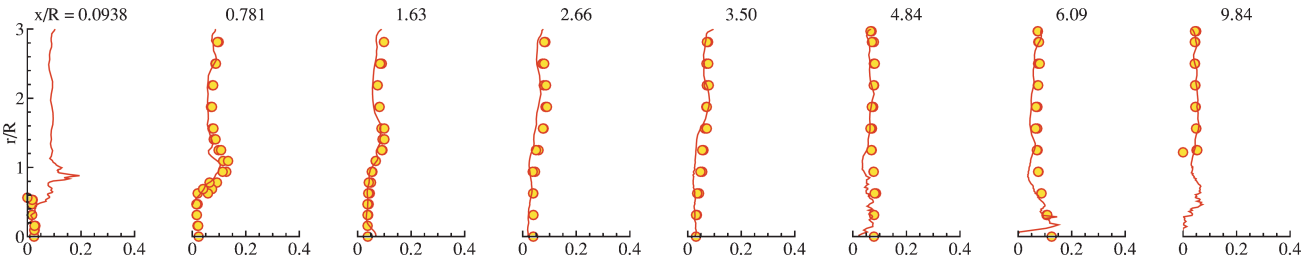

c) Azimuthal component

Fig. 13 RMS profiles of dimensionless particle-phase velocity field (case 2): ○, measured data from Refs. 42–44 and ——, LES results.

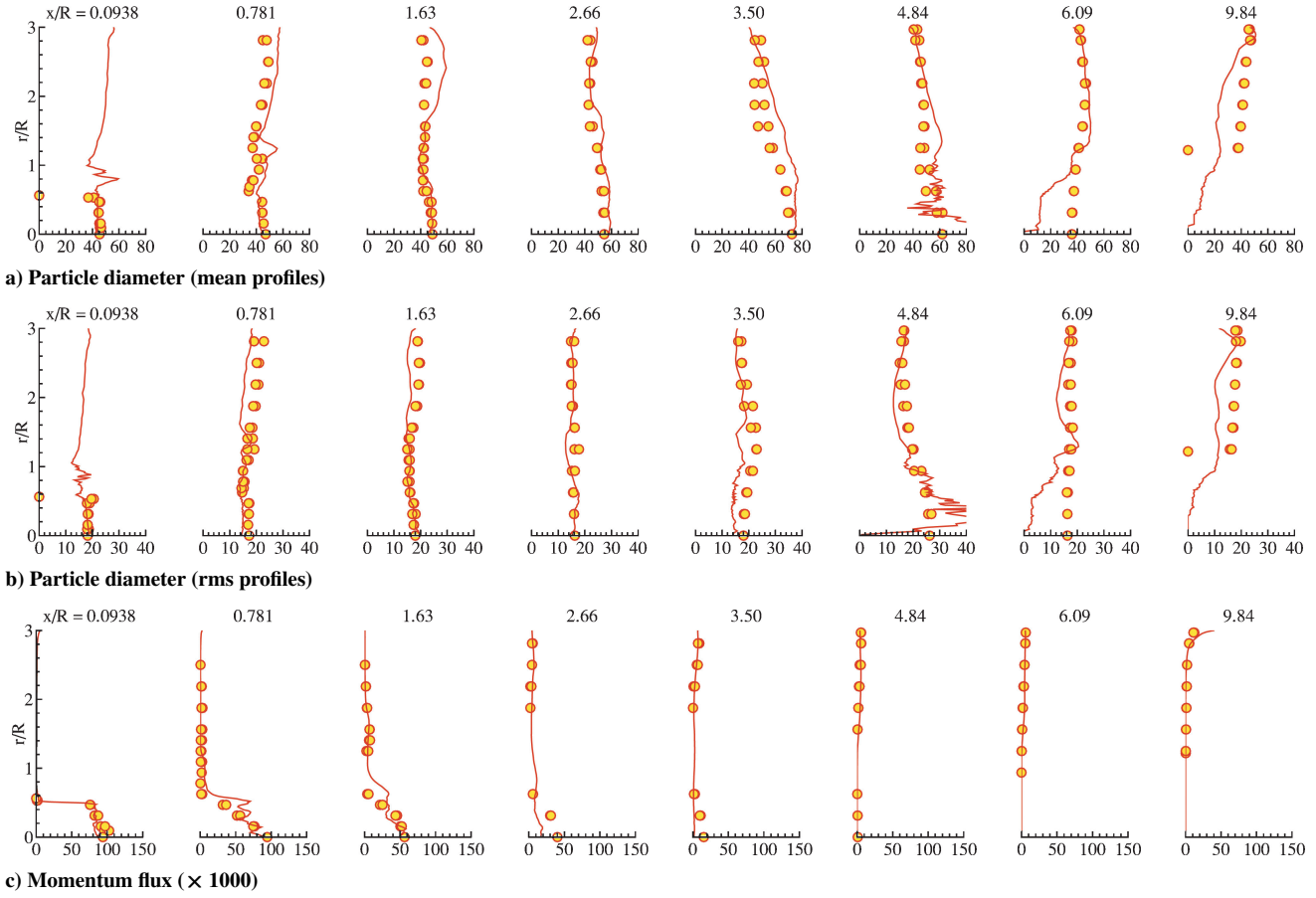

Fig. 14 Dimensionless particle diameter and momentum flux profiles (case 2): ○, measured data from Refs. 42–44 and ——, LES results.

those typically observed in gas-turbine combustors. It is impossible to address the more complex issues related to combustion in such flowfields without achieving this level of confidence first.

C. Validation of LES Combustion Processes for Gas-Turbine Applications

In the preceding sections we established the groundwork for simulating wall-bounded turbulent flow, nonreacting particle-laden flow, and recirculating swirl flow with characteristics relevant to gas-turbine combustors. We highlighted a systematic approach for validating the accuracy of LES in a progressive manner, with well-defined and carefully implemented boundary conditions. Each of these steps is a precursor toward validation of SGS models for reacting flows in gas turbines. In this section, we focus on recent work aimed at the validation of combustion models for LES in a similarly systematic manner. In doing so, we start with examples drawn from the International Workshop on Measurement and Computation of Turbulent Nonpremixed Flames (TNF)[1] and then look toward combustion modeling challenges that are central to gas-turbine applications but that have yet to be addressed systematically in the context of rigorous LES model validation.

Dynamic stability, low-emissions, reliability, and high-performance are key points associated with the design of most combustors. This is especially true in gas turbines due to simultaneously stringent requirements in all of these areas. The development of combustion models that can predict combustion in stratified mixtures, local extinction, ignition, and edge flame propagation is a critical consideration. Of equal importance for liquid-fueled systems is the development and validation of models for fuel atomization processes, secondary breakup, and spray combustion phenomena.

The TNF Workshop[1] is an ongoing collaboration among experimental and computational researchers. Its initial focus was on fundamental issues of turbulence–chemistry interaction in nonpremixed and partially premixed flames. A framework was established to facilitate detailed collaborative comparisons on measured and modeled results for a series of well-characterized target flames that carry through a systematic progression in the complexity of the combustion chemistry and flow dynamics. Starting with the simplest cases, experiments were designed to allow separate physical processes and individual submodels to be isolated. For example, a series of hydrogen jet flames with helium dilution allowed a detailed evaluation of NO predictions, independent of uncertainties in the radiation model.[48] Jet flames of $CO/H_2/N_2$ (Ref. 49) and $CH_4/N_2/H_2$ (Ref. 50) added kinetic complexity while maintaining the simple attached jet-flame geometry. The series of piloted CH_4–air jet flames[51] included increasing degrees of localized extinction that tests the ability of models to treat local extinction resulting from strong interactions of turbulence and chemistry. Turbulent flames stabilized by recirculation zones induced by bluff-bodies[52] or swirling flows[53] added fluid-dynamic complexity that is challenging to current models. Lifted jet flames in vitiated coflow[54] serve to isolate the mixing and chemistry dominated aspects of flame stabilization processes from the complex fluid dynamics of recirculating flows. Much of this work has involved RANS models, but there has been increasing emphasis on LES and on experiments directed specifically at validation of LES for combustion.

A central theme of the TNF series has been to use detailed comparisons of results from experiments and multiple modeling approaches to quantify state-of-the-art modeling capabilities and identify priorities for specific experimental and computational research needed to progress further toward predictive capability. The piloted CH_4–air jet flames, which were initially measured by Barlow and Frank[51] and have since been modeled by numerous groups (see TNF website[1] for references), provide an example of the progress that can be realized through closely coupled experimental and computational research on well-defined target flames. This series includes piloted flames with increasing jet Reynolds number (1.34×10^4, 2.24×10^4, 3.36×10^4, and 4.48×10^4 for flames C–F) and increasing

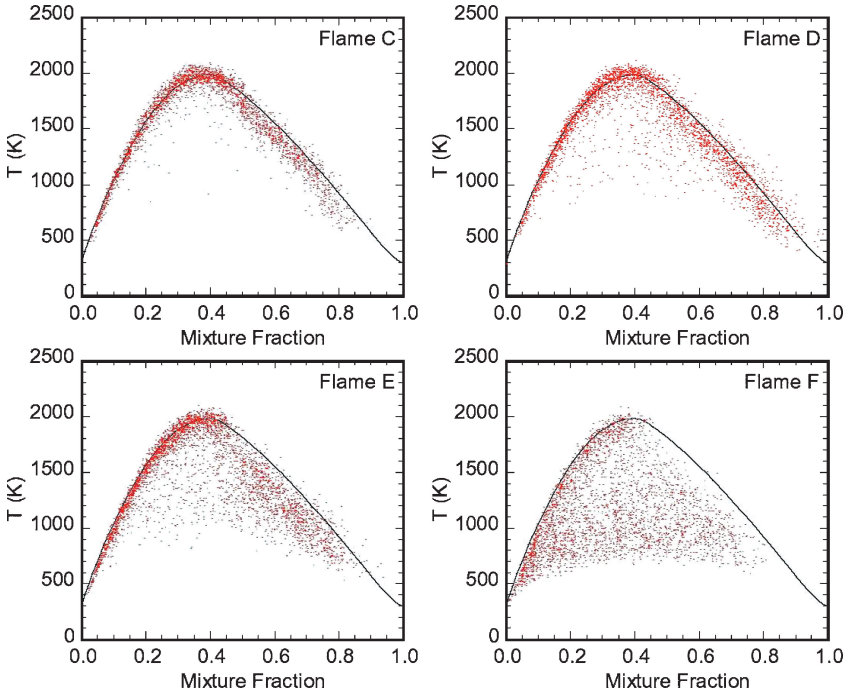

Fig. 15 Scatter plots of measured temperature at $x/d = 15$ in piloted CH_4–air jet flames by Barlow and Frank[51]; flames C, D, E, and F correspond to progressive increases in jet Reynolds number of 1.34×10^4, 2.24×10^4, 3.36×10^4, and 4.48×10^4.

probability of local extinction in the region above the pilot. The degree of extinction is shown in Fig. 15, which includes scatter plots of the measured temperature at $x/d = 15$ in each flame. The calculated temperature profile of an opposed-flow laminar flame with a strain of 50 s^{-1} is included to facilitate visual comparisons. Although several modeling approaches have been successful in matching the experimental velocity and scalar results for flame D, only the RANS-based PDF models[55,56] have so far accurately captured the progress of extinction in flames E and F. Thus, the modeling of local extinction and reignition represents an immediate challenge for LES.

Initial comparisons at TNF3 in 1998 were limited to flame D (very little extinction) and were based on multiscalar point measurements and two-component laser-Doppler-anemometer (LDA) measurements. Questions raised by those comparisons lead to experimental and computational investigations on the validity of chemical mechanisms[57] and radiation models[58,59] applied to these flames, with particular emphasis on the prediction of NO emissions. From the broader perspective, reliable and robust SGS models for predicting emissions do not exist. The relative performance of chemical kinetics mechanisms in predicting NO in methane flames largely depends on the degree of partial premixing. This situation is compounded by thermal radiation effects. The target flames studied under TNF typically have a low radiative heat loss. There are no clear conclusions or recommendations, however, with respect to radiation models, and this remains an open issue. There is evidence to suggest that the optically thin model is not accurate enough for the typical flames studied. The influence of flame radiation on major species mass fractions is not significant, but has been shown to reduce the predicted level of NO. The effects of turbulence–radiation interactions and, most importantly, the effect of temperature fluctuations, can have a measurable influence on the mean radiative energy.

More recent experimental research on these piloted flames has focused on scalar dissipation, scalar length scales, and spatial structure.[60,61] Scalar dissipation data are important for a wide range of modeling approaches, including flamelet- and CMC-based combustion models for LES. Structural information, such as length scales and flame orientation statistics, has the potential to be used directly in the validation of LES, and some initial comparisons of these quantities have been reported.[62] Therefore, even though these jet flames are relatively simple with regard to large-scale flow dynamics, they represent an important baseline for development and validation of LES combustion models.

Local extinction is just one of several challenging phenomena that must be addressed on the way to predictive LES capability for gas-turbine applications. Combustors typically use swirl to generated recirculation zones where hot combustion products serve to stabilize the flame in a region that is detached from surfaces. Combustion generally occurs in mixtures that are stratified to some degree. A robust model will be required to capture simultaneously these phenomena and more. However, the process of systematic validation is best pursued by first isolating these separate combustion phenomena and testing models against each aspect of the complete problem. A last key area pertinent to the robust prediction of combustion is the treatment of lifted flames. The Berkeley vitiated coflow burner (see Ref. 54) produces a lifted flame stabilized in a vitiated coflow. Practical burners use recirculation of combustion products to promote flame stabilization. The vitiated coflow burner was designed to examine flame stabilization in combustion products without the complexity of flow recirculation.

Lifted flames in vitiated coflows are receiving attention with a particular focus on autoignition as a stabilization mechanism. The Cabra configuration, which incorporates a large hot coflow, seems to have lifted modes where stabilization occurs by premixed flame propagation and autoignition modes where the flame is dominated by convection and reaction only. Flame stabilization in a nonuniformly mixed flow is also challenging model problem. Most turbulent burners are operated so that the flame is not in direct contact with hardware, that is, lifted. The lifted jet flame is an appropriate starting point for investigation of models that must eventually predict the flame stabilization details of more complicated burners. The progression of TNF Workshop target flames has already address some of these phenomena, including flow recirculation in the Sydney bluff-body flames (see Ref. 52) and swirling flames[53] and lifted flames stabilized in a coflow of combustion products.[54]

There is significant work still to be done to establish appropriate benchmark cases for validation of models for turbulent premixed combustion, including combustion of stratified mixtures. When the philosophy of systematic and rigorous validation expressed

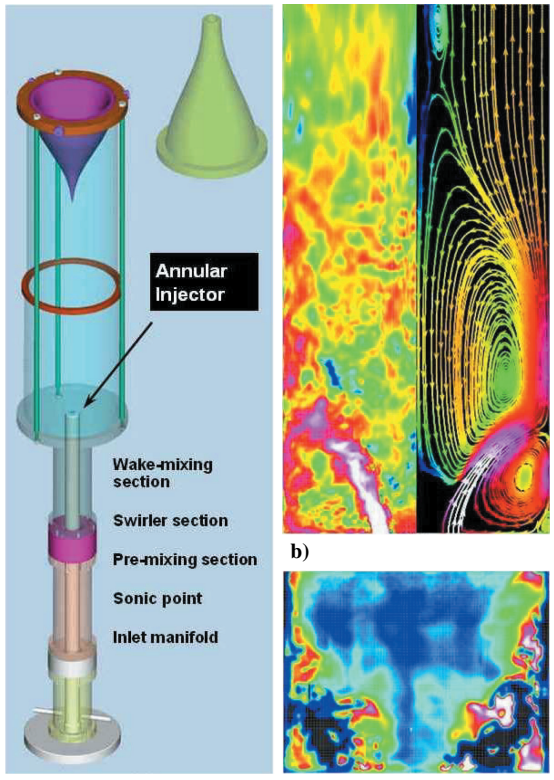

Fig. 16 CRF swirling-flow dump-combustor designed to study ultra-lean premixed combustion processes with emphasis on modeling and validation using LES: a) diagram of burner, b) instantaneous (left) and time-averaged (right) velocity fields from LES solution of baseline operating condition, and c) OH PLIF image that highlights flame structure at same baseline operating condition.

throughout this paper is followed, target cases for experimental validation of premixed combustion models must be developed with specific attention to the requirements for unambiguous boundary conditions, comprehensive and accurate measurements, and flame conditions that do not reach far beyond the expected capability of state-of-the-art models. As one example, experimental and computational work is currently in progress on the enclosed, atmospheric pressure, swirling, lean premixed dump combustor shown in Fig. 16. This burner was designed to study ultra-lean premixed combustion processes with emphasis placed on modeling and validation using LES. The design has been optimized to provide nonambiguous boundary conditions required for the validation of high-fidelity LES simulations, while making optimal use of the advanced laboratory and diagnostic capabilities developed at the Combustion Research Facility (CRF).

Figure 16a shows a diagram of the burner, including the injector section and two different types of exit nozzles, Fig. 16b a representative LES solution at the baseline operating condition that shows the instantaneous (left) and time-averaged (right) velocity field and Fig. 16c a representative OH planar-laser-induced-florescence (PLIF) image that shows the instantaneous flame structure at the same baseline operating condition. As was the case for the Refs. 42–44 configuration shown in Fig. 4, this burner produces two flow recirculation zones. One is located downstream of the centerbody and the other is located at the intersection of the vertical combustor wall and the horizontal inlet plate. At the conditions shown, flames are seen both downstream of the centerbody and in the corner recirculation zone. The corresponding OH PLIF image represents the variation in the OH mole fraction. The outer edge of the high-OH region is irregular and reflects variations in the local velocity, which contort the flame surface. The OH is uniform throughout much of the flame, with locally high concentration regions forming thin filaments that typically extend along the irregular interface located between unburned reactants and combustion products. By the use of high OH as an indicator of high temperature, the high-temperature region is continuous over a large area downstream of the upstream flame front. Preliminary LES calculations qualitatively produce the same trends. Activities in the area of premixed combustion at future TNF workshops will depend on the pace of experimental progress and the adoption of one or more target cases by modelers.

V. Conclusions

The results presented provide a systematic approach for the application and validation of the LES technique for gas-turbine combustion processes. Emphasis has been placed on boundary conditions and the progressive implementation toward more complex configurations. The discussion was formulated using the fundamental tradeoffs and requirements for LES as the central basis. A set of case studies were then presented using a single unified theoretical–numerical framework. First, the groundwork for simulating wall-bounded turbulent flow, nonreacting particle-laden flow, and complex swirling, recirculating flow typically observed in gas-turbine combustors was established. This groundwork was established by validating the accuracy of LES in a progressive manner, with well-defined and carefully implemented boundary conditions. Each of the steps taken represent precursors toward validation SGS models for reacting flows under well-defined conditions. The discussion then focused on issues related to combustion modeling. The goal was not to cite how various models and modeling approaches perform, but to provide a perspective on what all of the current models have not been able to predict reliably.

It is clear from the LES calculations presented to date that a wide variety of grid resolutions are being employed for the same types of cases. This disparity is primarily due to limited computational resources and the long turnaround times required when one uses denser (but preferable) grids. As research progresses, it will become imperative that grid resolution issues be addressed in a systematic way to establish the appropriate performance metrics and better separate numerical errors from modeling errors. The appropriate specification of boundary conditions is inherently coupled to the specification of grid resolution requirements and the related sensitivities. Ideally, future studies should address both issues simultaneously. Detailed analysis of the accuracy and sensitivities associated with LES SGS models, particularly those associated with turbulence–chemistry interactions, can only occur after a high level of confidence is established in our ability to simulate geometrically dominated turbulent fluid dynamic processes associated with the various target flames.

Because combustion occurs at the smallest scales, it will become more and more important to study subgrid turbulence–chemistry interactions with minimal ambiguities associated with both the experiments and companion calculations. To achieve this goal in the systematic manner described, it is imperative that the target flame descriptions include simultaneous velocity–scalar measurements with well-documented boundary conditions. Good progress has been made, and it will become more and more important to establish high-fidelity benchmarks that systematically focus on validation, boundary conditions, and treatment of complex flow dynamics at realistic conditions. In addition, research must be conducted to quantify the combined effect of noise, spatial averaging, and angle bias in the measurements of scalar dissipation, such that realistic uncertainty estimates may be provided.

Effects of turbulent mixing on reaction zone structures in nonpremixed and partially premixed flames have important implications for combustion models. In particular, a more complete understanding of the response of species mass fractions to turbulent mixing is needed to improve predictive capabilities. More detailed comparisons on measured and modeled results for scalar dissipation and related quantities are also required. Comparisons need to be extended back to aspects of the turbulent velocity and scalar fields, so that the reasons for the wide differences among predicted scalar dissipation profiles may be understood. To do this well, we will need to compare more than just scalar variance and scalar dissipation. The systematic progression of results in flow configurations designed for

closely coupled experimental and numerical research is essential to the development of robust, predictive, integrated models that have a solid basis in fundamental combustion science.

Acknowledgments

The U.S. Department of Energy, Office of Basic Energy Sciences, Division of Chemical Sciences, Geosciences, and Biosciences supported this work. Sandia National Laboratories is a multiprogram laboratory operated by the Sandia Corporation, a Lockheed Martin Company, for the U.S. Department of Energy under Contract DE-AC04-94-AL85000.

References

[1]Barlow, R. S., "International Workshop on Measurement and Computation of Turbulent Nonpremixed Flames," Combustion Research Facility, Sandia National Labs., Livermore, CA, URL: http://www.ca.sandia.gov/TNF [cited Nov. 2005].

[2]Oefelein, J. C., "General Numerical Framework for Reacting Multiphase Flow with Complex Thermochemistry, Thermodynamics and Transport," Sandia National Labs., SAND Rept. (to be published).

[3]Oefelein, J. C., "General Package for Evaluation of Multicomponent Real-Gas and Liquid Mixture States at All Pressures," Sandia National Labs., SAND Rept. (to be published).

[4]Erlebacher, G., Hussaini, M. Y., Speziale, C. G., and Zang, T. A., "Toward the Large Eddy Simulation of Compressible Turbulent Flows," *Journal of Fluid Mechanics*, Vol. 238, 1992, pp. 155–185.

[5]Speziale, C. G., "Galilean Invariance of Subgrid-Scale Stress Models in the Large Eddy Simulation of Turbulence," *Journal of Fluid Mechanics*, Vol. 156, 1985, pp. 55–62.

[6]Germano, M., Piomelli, U., Moin, P., and Cabot, W. H., "A Dynamic Subgrid-Scale Eddy Viscosity Model," *Physics of Fluids*, Vol. 3, No. 7, 1991, pp. 1760–1765.

[7]Moin, P., Squires, K., Cabot, W., and Lee, S., "A Dynamic Subgrid-Scale Model for Compressible Turbulence and Scalar Transport," *Physics of Fluids*, Vol. 3, No. 11, 1991, pp. 2746–2757.

[8]Lilly, D. K., "A Proposed Modification of the Germano Subgrid-Scale Closure Method," *Physics of Fluids*, Vol. 3, No. 11, 1992, pp. 633–635.

[9]Zang, Y., Street, R. L., and Koseff, J. R., "A Dynamic Mixed Subgrid-Scale Model and Its Application to Turbulent Recirculating Flows," *Physics of Fluids*, Vol. 5, No. 12, 1993, pp. 3186–3195.

[10]Vreman, B., Geurts, B., and Kuerten, H., "On the Formulation of the Dynamic Mixed Subgrid-Scale Model," *Physics of Fluids*, Vol. 6, No. 12, 1994, pp. 4057–4059.

[11]Smagorinsky, J., "General Circulation Experiments with the Primitive Equations. I. The Basic Experiment," *Monthly Weather Review*, Vol. 91, No. 3, 1963, pp. 99–164.

[12]Leland, T. W., and Chappelear, P. S., "The Corresponding States Principle. A Review of Current Theory and Practice," *Industrial and Engineering Chemistry Fundamentals*, Vol. 60, No. 7, 1968, pp. 15–43.

[13]Rowlinson, J. S., and Watson, I. D., "The Prediction of the Thermodynamic Properties of Fluids and Fluid Mixtures—I. The Principle of Corresponding States and Its Extensions," *Chemical Engineering Science*, Vol. 24, No. 8, 1969, pp. 1565–1574.

[14]Oefelein, J. C., "Simulation and Analysis of Turbulent Multiphase Combustion Processes at High Pressures," Ph.D. Dissertation, Dept. of Mechanical Engineering, Pennsylvania State Univ., University Park, PA, May 1997.

[15]Oefelein, J. C., and Yang, V., "Modeling High-Pressure Mixing and Combustion Processes in Liquid Rocket Engines," *Journal of Propulsion and Power*, Vol. 14, No. 5, 1998, pp. 843–857.

[16]Reid, R. C., Prausnitz, J. M., and Polling, B. E., *The Properties of Liquids and Gases*, 4th ed., McGraw–Hill, New York, 1987, Chaps. 3 and 5.

[17]VanWylen, G. J., and Sonntag, R. E., *Fundamentals of Classical Thermodynamics*, 3rd ed., Wiley, New York, 1986, Chap. 10.

[18]Gordon, S., and McBride, B. J., "Computer Program for Calculation of Complex Chemical Equilibrium Compositions, Rocket Performance, Incident and Reflected Shocks and Chapman-Jouguet Detonations," NASA SP-273, 1971.

[19]Kee, R. J., Rupley, F. M., and Miller, J. A., "Chemkin Thermodynamic Data Base," Sandia National Lab., Technical Rept. SAND87-8215B, Livermore, CA, 1990.

[20]Ely, J. F., and Hanley, H. J. M., "Prediction of Transport Properties. 1. Viscosity of Fluids and Mixtures," *Industrial and Engineering Chemistry Fundamentals*, Vol. 20, No. 4, 1981, pp. 323–332.

[21]Ely, J. F., and Hanley, H. J. M., "Prediction of Transport Properties. 2. Thermal Conductivity of Pure Fluids and Mixtures," *Industrial and Engineering Chemistry Fundamentals*, Vol. 22, No. 1, 1981, pp. 90–97.

[22]Bird, R. B., Stewart, W. E., and Lightfoot, E. N., *Transport Phenomena*, Wiley, New York, 1960.

[23]Hirschfelder, J. O., Curtiss, C. F., and Bird, R. B., *Molecular Theory of Gases and Liquids*, 2nd ed., Wiley, New York, 1964.

[24]Takahashi, S., "Preparation of a Generalized Chart for the Diffusion Coefficients of Gases at High Pressures," *Journal of Chemical Engineering of Japan*, Vol. 7, No. 6, 1974, pp. 417–420.

[25]Peters, N., "Laminar Diffusion Flamelet Models in Non-Premixed Turbulent Combustion," *Progress in Energy and Combustion Science*, Vol. 10, No. 3, 1984, pp. 319–339.

[26]Peters, N., *Turbulent Combustion*, Cambridge Univ. Press, Cambridge, England, U.K., 2000.

[27]Klimenko, A. Y., "Multicomponent Diffusion of Various Scalars in Turbulent Flow," *Fluid Dynamics*, Vol. 25, 1990, pp. 327–334.

[28]Bilger, R. W., "Conditional Moment Closure for Turbulent Reacting Flow," *Physics of Fluids*, Vol. 5, No. 2, 1993, pp. 436–444.

[29]Klimenko, A. Y., and Bilger, R. W., "Conditional Moment Closure for Turbulent Combustion," *Progress in Energy and Combustion Science*, Vol. 25, No. 6, 1999, pp. 595–687.

[30]Pope, S. B., "PDF Methods for Turbulent Reactive Flows," *Progress in Energy and Combustion Science*, Vol. 11, No. 2, 1985, pp. 119–192.

[31]Givi, P., "Model Free Simulations of Turbulent Reactive Flows," *Progress in Energy and Combustion Science*, Vol. 15, No. 1, 1989, pp. 1–107.

[32]Colucci, P. J., Jaberi, F. A., Givi, P., and Pope, S. B., "Filtered Density Function for Large Eddy Simulation of Turbulent Reacting Flows," *Physics of Fluids*, Vol. 10, No. 2, 1998, pp. 499–515.

[33]Jaberi, F. A., Colucci, P. J., James, S., Givi, P., and Pope, S. B., "Filtered Mass Density Function for Large Eddy Simulation of Turbulent Reacting Flows," *Journal of Fluid Mechanics*, Vol. 401, 1999, pp. 85–121.

[34]Klimenko, A. Y., "On the Relation Between the Conditional Moment Closure and Unsteady Flamelets," *Combustion Theory and Modelling*, Vol. 5, 2001, pp. 275–294.

[35]Pantano, C., and Sarkar, S., "A Subgrid Model for Nonlinear Functions of a Scalar," *Physics of Fluids*, Vol. 13, No. 12, 2001, pp. 3803–3819.

[36]Mellado, J. P., Sarkar, S., and Pantano, C., "Reconstruction Subgrid Models for Nonpremixed Combustion," *Physics of Fluids*, Vol. 15, No. 11, 2003, pp. 3280–3307.

[37]Colin, O., Ducros, F., Veynante, D., and Poinsot, T., "A Thickened Flame Model for Large Eddy Simulation of Turbulent Premixed Combustion," *Physics of Fluids*, Vol. 12, No. 7, 2000, pp. 1843–1863.

[38]Chakravarthy, V. K., and Menon, S., "Large Eddy Simulation of Turbulent Premixed Flames in the Flamelet Regime," *Combustion Science and Technology*, Vol. 162, 2001, pp. 175–222.

[39]Kerstein, A. R., "A Linear Eddy Model of Turbulent Scalar Transport and Mixing," *Combustion Science and Technology*, Vol. 60, 1988, pp. 391–421.

[40]Kerstein, A. R., "One-Dimensional Turbulence: Model Formulation and Application to Homogeneous Turbulence, Shear Flows, and Buoyant Stratified Flows," *Journal of Fluid Mechanics*, Vol. 392, 1999, pp. 277–334.

[41]Moser, R. D., Kim, J., and Mansour, N. N., "Direct Numerical Simulation of Turbulent Channel Flow up to $Re_\tau = 590$," *Physics of Fluids*, Vol. 11, No. 4, 1999, pp. 943–945.

[42]Sommerfeld, M., and Qiu, H. H., "Detailed Measurements in a Swirling Particulate Two-Phase Flow by a Phase-Doppler Anemometer," *International Journal of Heat and Fluid Flow*, Vol. 12, No. 1, 1991, pp. 20–28.

[43]Sommerfeld, M., Ando, A., and Wennerberg, D., "Swirling, Particle-Laden Flows Through a Pipe Expansion," *Journal of Fluids Engineering*, Vol. 114, 1992, pp. 648–656.

[44]Sommerfeld, M., and Qiu, H. H., "Characterization of Particle-Laden, Confined Swirling Flows by Phase-Doppler Anemometry and Numerical Calculation," *International Journal of Multiphase Flow*, Vol. 19, No. 6, 1993, pp. 1093–1127.

[45]Crowe, C. T., Sharma, M. P., and Stock, D. E., "The Particle-Source-In-Cell (PSI-CELL) Model for Gas-Droplet Flows," *Journal of Fluids Engineering*, Vol. 99, 1977, pp. 325–332.

[46]Clift, R., Grace, J. R., and Weber, M. E., *Bubbles, Drops, and Particles*, Academic Press, New York, 1978.

[47]Segura, J. C., Eaton, J. K., and Oefelein, J. C., "Predictive Capabilities of Particle-Laden Large Eddy Simulation," Dept. of Mechanical Engineering, Technical Rept. TSD-156, Stanford Univ., Stanford, CA, 2004.

[48]Barlow, R. S., Smith, N. S. A., Chen, J. Y., and Bilger, R. W., "Nitric Oxide Formation in Dilute Hydrogen Jet Flames: Isolation of the Effects of Radiation and Turbulence-Chemistry Submodels," *Combustion and Flame*, Vol. 117, 1999, pp. 4–31.

[49]Barlow, R. S., Fiechtner, G. J., Carter, C. D., and Chen, J. Y., "Experiments on the Structure of Turbulent $CO/H_2/N_2$ Jet Flames," *Combustion and Flame*, Vol. 120, 2000, pp. 549–569.

[50]Meier, W., Barlow, R. S., Chen, Y. L., and Chen, J. Y., "Raman/Rayleigh/LIF Measurements in a Turbulent $CH_4/H_2/N_2$ Jet Diffusion Flame: Experimental Techniques and Turbulence Chemistry Interaction," *Combustion and Flame*, Vol. 123, 2000, pp. 326–343.

[51]Barlow, R. S., and Frank, J. H., "Effects of Turbulence on Species Mass Fractions in Methane/Air Jet Flames," *Proceedings of the Combustion Institute*, Vol. 27, No. 1, 1998, pp. 1087–1095.

[52]Dally, B. B., Masri, A. R., Barlow, R. S., and Fiechtner, G. J., "Instantaneous and Mean Compositional Structure of Bluff-Body Stabilized Nonpremixed Flames," *Combustion and Flame*, Vol. 114, 1998, pp. 119–148.

[53]Kalt, P. A., Al-Abdeli, Y. M., Masri, A. R., and Barlow, R. S., "Swirling Turbulent Non-Premixed Flames of Methane: Flow Field and Compositional Structure," *Proceedings of the Combustion Institute*, Vol. 29, No. 2, 2002, pp. 1913–1919.

[54]Cabra, R., Myhrvold, T., Chen, J. Y., Dibble, R. W., Karpetis, A. N., and Barlow, R. S., "Simultaneous Laser Raman-Rayleigh-LIF Measurements and Numerical Modeling Results of a Lifted Turbulent H_2/N_2 Jet Flame in a Vitiated Coflow," *Proceedings of the Combustion Institute*, Vol. 29, No. 2, 2002, pp. 1881–1888.

[55]Xu, J., and Pope, S. B., "PDF Calculations of Turbulent Nonpremixed Flames with Local Extinction," *Combustion and Flame*, Vol. 123, 2000, pp. 281–307.

[56]Lindstedt, R. P., Louloudi, S. A., Vaos, E. M., and Bilger, R. W., "Joint Scalar Probability Density Function Modeling of Pollutant Formation in Piloted Turbulent Jet Diffusion Flames with Comprehensive Chemistry," *Proceedings of the Combustion Institute*, Vol. 28, No. 1, 2000, pp. 149–156.

[57]Barlow, R. S., Karpetis, A. N., and Frank, J. H., "Scalar Profiles and NO Formation in Laminar Opposed-Flow Partially Premixed Methane/Air Flames," *Combustion and Flame*, Vol. 127, 2001, pp. 2102–2118.

[58]Frank, J. H., Barlow, R. S., Lundquist, C., and Pope, S. B., "Radiation and Nitric Oxide Formation in Turbulent Non-Premixed Jet Flames," *Proceedings of the Combustion Institute*, Vol. 28, No. 1, 2000, pp. 447–454.

[59]Coelho, P. J., Teerling, O. J., and Roekaerts, D., "Spectral Radiative Effects and Turbulence/Radiation Interaction in a Non-Luminous Turbulent Jet Diffusion Flame," *Combustion and Flame*, Vol. 133, 2003, pp. 75–91.

[60]Karpetis, A. N., and Barlow, R. S., "Measurements of Flame Orientation and Scalar Dissipation in Turbulent Partially Premixed Methane Flames," *Proceedings of the Combustion Institute*, Vol. 30, No. 1, 2004, pp. 665–672.

[61]Barlow, R. S., and Karpetis, A. N., "Scalar Length Scales and Spatial Averaging Effects in Turbulent Piloted Methane/Air Jet Flames," *Proceedings of the Combustion Institute*, Vol. 30, No. 1, 2004, pp. 673–680.

[62]Kempf, A., Flemming, F., and Janicka, J., "Investigation of Lengthscales, Scalar Dissipation, and Flame Orientation in a Piloted Diffusion Flame by LES," *Proceedings of the Combustion Institute*, Vol. 30, No. 1, 2004, pp. 557–565.

F. Grinstein
Guest Editor

Color reproductions courtesy of Sandia National Laboratories.